

MARTIN MARIETTA ENERGY SYSTEMS LIBRARIES



3 4456 0324859 0

ORNL/TM-11620

ornl

**OAK RIDGE
NATIONAL
LABORATORY**

MARTIN MARIETTA

Review of Recent Stellarator Results in the U.S.A., the U.S.S.R., and Japan

J. F. Lyon

OAK RIDGE NATIONAL LABORATORY
CENTRAL RESEARCH LIBRARY
CIRCULATION SECTION
4100 FORD ST.
LIBRARY LOAN COPY
DO NOT TRANSFER TO ANOTHER PERSON
If you wish someone else to use this
report, send to us with report and
the library will arrange a loan.

OPERATED BY
MARTIN MARIETTA ENERGY SYSTEMS, INC.
FOR THE UNITED STATES
DEPARTMENT OF ENERGY

This report has been reproduced exactly from the best available copy.

Available to DOD and DOD contractors from the Office of Scientific and Technical Information, P.O. Box 02, Oak Ridge, TN 37831; prices available from (615) 576-8401, FTS 626 8401.

Available to the public from the National Technical Information Service, U.S. Department of Commerce, 5305 North Royal Road, Springfield, VA 22161.

This report was prepared as a part of work sponsored by an agency of the United States Government. Neither the United States Government nor any agency thereof, nor any of its employees, makes any warranty, express or implied, or assumes any liability for or responsibility for the accuracy, completeness, or usefulness of any information, apparatus, product, or process disclosed, or represents that its use would infringe privately owned rights. Reference herein to any specific commercial product, process, or service by trade name, trade name, or otherwise, does not necessarily constitute or imply its endorsement, recommendation, or approval by the United States Government or any agency thereof. The views and opinions of authors expressed herein do not necessarily state or reflect those of the United States Government or any agency thereof.

ORNL/TM-11620
Dist. Category UC-426

Fusion Energy Division

**REVIEW OF RECENT STELLARATOR RESULTS
IN THE U.S.A., THE U.S.S.R., AND JAPAN**

J. F. Lyon

Date published: December 1990

Prepared for the
Office of Fusion Energy
Budget Activity No. AT 10 10 15 B

Prepared by the
OAK RIDGE NATIONAL LABORATORY
Oak Ridge, Tennessee 37831-6285
managed by
MARTIN MARIETTA ENERGY SYSTEMS, INC.
for the
U.S. DEPARTMENT OF ENERGY
under contract DE-AC05-84OR21400



3 4456 0324859 0

CONTENTS

ABSTRACT	v
1. INTRODUCTION	1
2. MAGNETIC CONFIGURATION OPTIMIZATION	2
3. SUMMARY OF RECENT PERFORMANCE	4
4. MAGNETIC SURFACE STUDIES	6
4.1 Magnetic Field Errors	6
4.2 Bootstrap Currents	8
5. TRAPPED-PARTICLE LOSSES	9
6. FINITE-BETA BEHAVIOR	12
6.1 Maximum Beta Values	12
6.2 Second Stability Behavior	13
7. GLOBAL CONFINEMENT	16
8. LOCAL TRANSPORT STUDIES	19
9. FLUCTUATION STUDIES	21
10. PARTICLE AND IMPURITY CONTROL	24
11. CONCLUSIONS	25
ACKNOWLEDGMENTS	28
REFERENCES	29

ABSTRACT

Stellarators with significant magnetic shear in the United States, the Soviet Union, and Japan are described, and recent results are discussed in terms of their contributions to the physics understanding relevant for stellarator optimization and to toroidal confinement understanding in general. The areas discussed are the properties of stellarators with significant shear, magnetic surfaces, trapped-particle losses, magnetohydrodynamic (MHD) stability, global confinement scaling, local transport, fluctuations, and particle and impurity control.

1. INTRODUCTION

The period covered by this review, January 1989 to June 1990, has been a productive time in the world stellarator program. Three major experiments that began operation in 1988 have produced significant results: the Advanced Toroidal Facility (ATF) (Lyon *et al.*, 1990a) at Oak Ridge, U.S.A.; the Compact Helical System (CHS) (Nishimura *et al.*, 1990) at Nagoya, Japan; and Wendelstein VII-AS (Sapper and Renner, 1990) at Garching, F.R.G. In addition, important results were obtained during this period from older experiments: L-2 (L-2 Team and ECR Group, 1989), operating since 1975 at Moscow, U.S.S.R.; Heliotron E (Obiki *et al.*, 1990a), operating since 1980, and Heliotron DR (Morimoto *et al.*, 1989), operating since 1981, at Kyoto, Japan; Uragan-3 (Berezhnyi *et al.*, 1989), operating since 1981 at Kharkov, U.S.S.R.; and the Interchangeable Module Stellarator (IMS) (Shohet and the TSL Group, 1990), operating since 1984 at Madison, U.S.A. Earlier work has been reviewed elsewhere (Carreras *et al.*, 1988; Kovrizhnykh, 1988).

Stellarator research is primarily aimed at developing physics understanding in support of the development of large, next-generation experiments (Lyon, 1990b) and of a more attractive steady-state reactor concept. However, stellarator research can also contribute to better understanding of tokamaks. Both belong to the family of toroidal confinement devices characterized by helical (toroidal plus poloidal) magnetic fields that form toroidally nested, closed magnetic surfaces. Stellarators complement tokamaks in their magnetic configuration properties (absence of a net toroidal plasma current, generally opposite sign of magnetic shear, nonaxisymmetry, etc.) and in better external control of these properties.

Stellarators encompass a wide range of currentless magnetic configurations. Three important properties characterizing these configurations are the rotational transform ι ($= 1/q$, where q is the tokamak safety factor), the global magnetic shear $\{= [\iota(\bar{a}) - \iota(0)]/\iota(0)$, where \bar{a} is the average radius of the inherently non-circular (and nonaxisymmetric) stellarator plasma}, and the size of the magnetic well (or hill). There are two major stellarator classifications: low-shear stellarators with a global magnetic well encompassing the entire plasma that are discussed elsewhere (Ringle *et al.*, 1990; Shi *et al.*, 1988), and higher-shear stellarators with a central magnetic well that predominate in the U.S.A., the U.S.S.R., and Japan. Recent results and progress (and preparations) toward better understanding and optimization of the latter class of devices are the subject of this review.

After a discussion of stellarators with shear (Sect. 2) and a description of the recent performance of these devices (Sect. 3), this review focuses on recent progress in addressing the following key issues for configuration optimization.

- (1) The shear common to these devices provides a stabilizing term for MHD instabilities. However, it also introduces a set of low-order rational values of ι into the plasma volume that can produce magnetic islands or broken magnetic surfaces in the presence of resonant error fields. Creation, correction, and avoidance of magnetic islands are discussed in Sect. 4. This section also contains an examination of the bootstrap current, which could change the magnetic configuration from the optimized one.

- (2) The helical windings used to create these magnetic configurations lead to large helical ripple and to a large population of helically trapped particles, which can give rise to instabilities (trapped-electron modes), higher neoclassical transport ($\chi \propto 1/\nu$ at lower collisionality), and direct collisionless loss (unconfined orbits) of helically trapped particles with small v_{\parallel}/v . Here χ is the heat diffusivity, ν is the collision frequency, and v_{\parallel} is the component of the particle velocity v parallel to \vec{B} . Flexible poloidal field coil sets can ameliorate these effects, and the ambipolar radial electric field can reduce the neoclassical transport and direct losses. These effects, particularly the loss of energetic helically trapped particles, are discussed in Sect. 5.
- (3) The other main component of configuration optimization is MHD stability and access to the second stability regime resulting from the finite-beta shift of the magnetic axis; this is discussed in Sect. 6.
- (4) The balance between confinement and beta in the optimization is reflected in the global confinement scaling studies described in Sect. 7, where a comparison with tokamak scaling is made.
- (5) Profiles, local transport, deviation from neoclassical transport, and the ambipolar electric field are discussed in Sect. 8. Studies of fluctuations and their correlation with transport are described in Sect. 9.
- (6) Particle and impurity control is important for steady-state operation and is discussed in Sect. 10.

Section 11 summarizes recent results in these areas and the steps needed to improve physics understanding for optimization of stellarators with shear.

2. MAGNETIC CONFIGURATION OPTIMIZATION

Magnetic configuration optimization is the key challenge for both the present and the next generation of stellarators with shear. It involves finding the optimum combination of configuration parameters (rotational transform, shear, poloidal field shaping, toroidal field component, helical ripple, etc.) that provides the best compromise among possibly conflicting requirements for high-beta operation (MHD equilibrium and stability limits), good confinement of energetic ions [such as those created with ion cyclotron range of frequency (ICRF) heating or perpendicular neutral beam injection (NBI)], low transport losses, good particle and impurity control, low bootstrap current generation, etc.

The stellarators discussed here generally rely on the outward shift of the magnetic axis with increasing beta to deepen an existing (vacuum) magnetic well that produces, in combination with the strong edge shear, a beta self-stabilization effect that permits access to a higher-beta second stability regime (Shafranov, 1983). This MHD optimization has led to increasingly lower plasma aspect ratio: $R/\bar{a} = 11$ (Heliotron E), 7–8 [ATF, the Large Helical Device (LHD)], 5 (CHS), and 3–4 (Compact Torsatrons) (Carreras *et al.*, 1987). However, an outward shift worsens orbit confinement and neoclassical transport. Reconciling the different requirements is the major challenge in configuration optimization for stellarators with shear.

The main configuration controls used in these devices are an additional toroidal field (Heliotron E, Uragan-2M) to change ϵ and shear, horizontal shifting of the vacuum magnetic axis (Heliotron E, ATF, CHS) to change the vacuum magnetic well (or hill), and poloidal field shaping (quadrupole component in ATF) to change the central value of ϵ and the fraction of the trapped particles that are confined.

The main device parameters for the experiments whose results are reviewed here are given in Table 1. Although these stellarators, currently the world's largest, are modest by present tokamak standards, this situation is expected to change when LHD comes into operation in 1997. This large next-generation experiment, now under design in Japan (Iiyoshi *et al.*, 1990), will have double the size and field of ATF (the largest of the present stellarators), an order of magnitude more heating power, and superconducting coils for steady-state operation.

Most of the devices considered here (ATF, CHS, Heliotron E, Heliotron DR, and Uragan-3M) produce the helical field by unidirectional currents in helical windings without the need for additional toroidal field (TF) coils, although such coils may be included for additional configuration flexibility (as on Heliotron E). In Uragan-2M and L-2, TF coils provide the bulk of the main field. Figure 1 illustrates the helical winding geometry and the poloidal field coil sets for CHS; ATF and LHD have a similar geometry, but are larger in scale by factors of two and four, respectively. The poloidal field coil sets are used to control the net plasma current (usually zero), the magnetic axis position, and the plasma shape [or $\epsilon(0)$] through the total flux, the dipole component, and the quadrupole component of the poloidal field, respectively. External control of the magnetic configuration with these coil sets provides a useful toroidal research tool for controlled study of the bootstrap current (Sect. 4.2), the dissipative trapped-electron mode (Sect. 5), and the second stability regime (Sect. 6.2), all topics of interest for tokamaks.

These devices form a complementary set: there are significant differences [aspect ratio, $\epsilon(r)$, well depth, etc.] within this set and between these devices

Table 1. Major device parameters for stellarators discussed in this review

Name	Location	Start of Operation	Major radius R_0 (m)	Minor radius \bar{a} (m)	B_0 (T), ^a Δt (s) ^b	P (MW), ^c Δt (s) ^b
Operating						
ATF	Oak Ridge, U.S.A.	1988	2.1	0.27	2.0, 5	2.2, 0.3
Heliotron E	Kyoto, Japan	1980	2.2	0.2	2.0, 0.5	5, 0.2
CHS	Nagoya, Japan	1988	1.0	0.2	1.5, 1	1.2, 1
L-2	Moscow, U.S.S.R.	1975	1.0	0.11	1.3	0.5, 0.01
Uragan-3M	Kharkov, U.S.S.R.	1981	1.0	0.11	2, 0.5	0.6, 0.05
Heliotron DR	Kyoto, Japan	1981	0.9	0.07	0.6	0.2, 0.01
Planned						
Uragan-2M	Kharkov, U.S.S.R.	1991	1.7	0.22	2.4, 2	6.2, 0.3
LHD	Toki, Japan	1997	4.0	0.5-0.6	4.0, ∞	≈ 30 , 10

^a B_0 = on-axis field.

^b Δt = pulse length at the maximum value of B_0 or P .

^c P = auxiliary heating power.

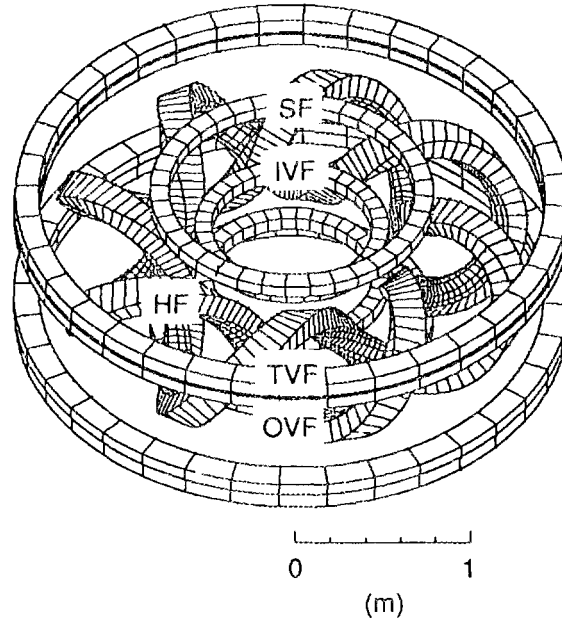


Fig. 1. Set of helical field (HF) windings and poloidal field coils on CHS: SF = shaping field, IVF = inner vertical field, TVF = trim vertical field, and OVF = outer vertical field.

and the low-shear stellarators. Three of the experiments (CHS, ATF, and L-2) and the LHD have generally similar magnetic configuration properties. They typically have $\iota(0) \sim 1/3$ and $\iota(\bar{a}) \sim 1$, just the opposite to tokamaks, in which typically $\iota(0) \sim 1$ and $\iota(\bar{a}) \sim 1/3$. The high-transform [$\iota(\bar{a}) = 2.5$] Heliotron E and the low-transform [$\iota(\bar{a}) \simeq 0.3$] Uragan-3M are complementary to this set. This complementarity is useful in understanding the effect of configuration changes. For example, the additional toroidal field on Heliotron E changes the ratio of toroidal to poloidal fields and hence $\iota(r)$, but it also changes \bar{a} , the plasma-wall distance, the plasma ellipticity, and the magnetic well (or hill).

3. SUMMARY OF RECENT PERFORMANCE

The relevance of the physics developed on the present generation of stellarators increases with increased device capability. Most of the results reviewed here were obtained on three experiments: ATF, CHS, and Heliotron E. These experiments have $R_0 \simeq 2$ m, $\bar{a} = 0.1$ – 0.27 m, $B_0 \leq 2$ T, $P_{ECH} = 0.4$ – 1 MW with pulse length ≤ 3.3 s, and $P_{NBI} = 1.2$ – 2 MW with pulse length ≤ 1 s. Substantial progress has been made during the period, in part because ATF and CHS are relatively new (1988) experiments and their capabilities are still expanding. In addition to increases in plasma parameters on ATF and CHS, there has been increased emphasis

on more sophisticated diagnostics and on extension of device capabilities for better understanding of different aspects of plasma behavior both in the new experiments and in the more mature Heliotron E, L-2, and Uragan-3M.

A typical discharge is shown in Fig. 2. Here electron cyclotron heating (ECH) is used to form a currentless plasma target in ATF for subsequent NBI. ICRF has been used for this purpose on CHS and on the Uragan torsatrons at Kharkov, allowing a wider range of magnetic field values. The plasma density and stored energy reach a stationary state in Fig. 2; the plasma duration is limited only by the heating pulse length. Longer (≈ 850 ms) stationary discharges have been obtained on CHS with a longer NBI pulse.

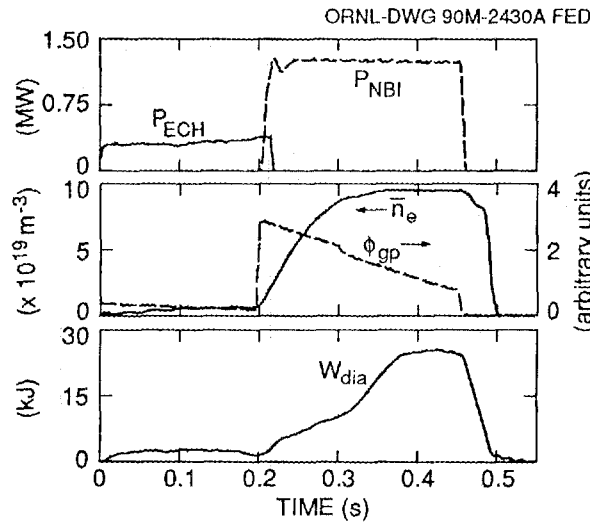


Fig. 2. ATF discharge history with NBI into an ECH target plasma at $B_0 = 1.9$ T. The gas puff rate is indicated by ϕ_{gp} and the diamagnetic loop measurement of the stored plasma energy by W_{dia} .

Parameter improvements on ATF are the result of operation at full field with higher power and with more effective gettering ($\approx 70\%$ coverage) of the vacuum vessel walls (Murakami *et al.*, 1990a). The maximum magnetic field increased from 1 T to 2 T and the total plasma heating power increased from ≈ 1 MW to 2 MW during this period. As a result, W_p increased from 8 kJ to 27 kJ, \bar{n}_e increased from $3.5 \times 10^{19} \text{ m}^{-3}$ to $1.2 \times 10^{20} \text{ m}^{-3}$, τ_E increased from ≈ 5 ms to ≈ 30 ms (at $P_{NBI} \approx 1$ MW), $\langle \beta \rangle$ increased from 0.5% to 1.5%, and the discharge duration increased from 1 s to 3.3 s for ECH alone and from < 0.1 s to 0.35 s (the full duration of the beam pulse) with NBI. The parameters obtained on CHS (Matsuoka *et al.*, 1990) are $T_e(0) \approx 1$ keV at $n_e(0) = 2 \times 10^{18} \text{ m}^{-3}$ and $T_e(0) \approx 500$ eV at $n_e(0) = 10^{19} \text{ m}^{-3}$ with only 50–100 kW of ECH at 53.2 GHz or 28 GHz, and $T_e(0) \approx 500$ eV at $n_e(0) \approx 2 \times 10^{19} \text{ m}^{-3}$ and $T_e(0) \approx 300$ eV at $n_e(0) \approx 10^{20} \text{ m}^{-3}$ with 400–950 kW of 35- to 40-kV NBI.

The maximum parameters obtained thus far are plasma stored energy $W_p = 27\text{--}34$ kJ, volume-average beta $\langle\beta\rangle = 1.5\text{--}2\%$, global energy confinement time $\tau_E = 20\text{--}30$ ms, line-average density $\bar{n}_e = 1\text{--}1.8 \times 10^{20} \text{ m}^{-3}$, central electron temperature $T_e(0) \leq 1\text{--}2.4$ keV, central ion temperature $T_i(0) \leq 1.6$ keV, $Z_{\text{eff}} \lesssim 2$, and $P_{\text{radiation}}/P_{\text{input}} \lesssim 30\%$. Figure 3 shows the parameter range obtained on the oldest and most developed of these devices, Heliotron E (Sudo *et al.*, 1990a). These parameters, and those in ATF and CHS, are comparable to those obtained in similar-scale tokamaks and allow relevant physics studies.

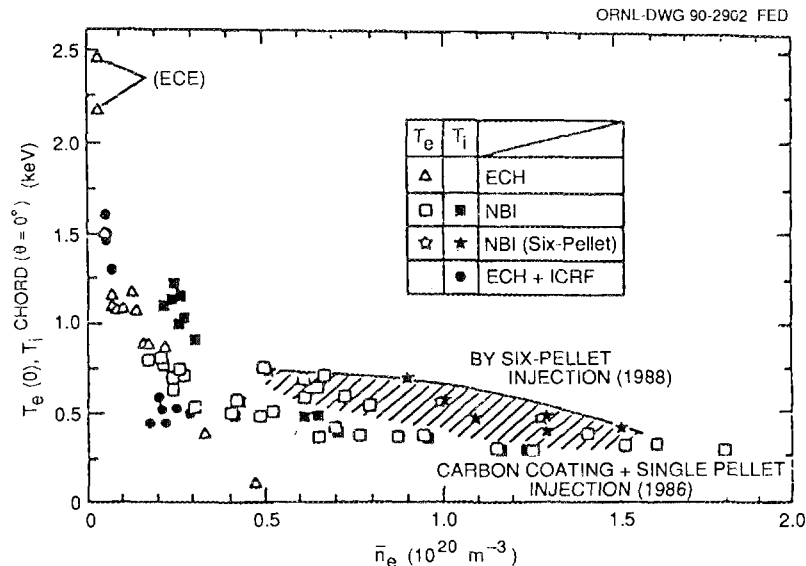


Fig. 3. Parameters obtained in Heliotron E with ECH, NBI, and ICRF heating. The highest electron temperatures are measured with electron cyclotron emission (ECE). The other $T_e(0)$ values are obtained from Thomson scattering. The $T_i(0)$ values are from the central chord of a neutral particle analyzer.

4. MAGNETIC SURFACE STUDIES

4.1 Magnetic Field Errors

Stellarators should have good vacuum magnetic surfaces because they do not require a net toroidal plasma current to produce the confining poloidal field. Ensuring the existence of good magnetic surfaces is the first step in magnetic configuration optimization. However, resonant field perturbations (field errors) can produce magnetic islands, which, if large enough, can reduce the plasma size. Magnetic surface mapping on Heliotron E using a resistivity method (Sudo, 1990) shows a fine structure (several subpeaks of the resistivity within a width of 7–8 cm) just inside the outermost magnetic surface, which may be due to ergodicity at $\nu \geq 2$. In ATF,

good agreement was obtained between islands measured with an electron beam and those calculated from field errors due to the current feeds to the helical and vertical field coils (Colchin *et al.*, 1989). This field perturbation was used to advantage to access the second stability region at lower beta than otherwise possible (Harris *et al.*, 1989); the field errors were then corrected (Colchin *et al.*, 1989). Field errors have also been corrected and additional poloidal coils installed for configuration flexibility on Uragan-3 (renamed Uragan-3M). The average plasma radius has increased from ≤ 9 cm to 11 cm, and the on-axis field capability has increased from ≤ 1 T to 2 T (Berezhnyi *et al.*, 1990).

Careful attention to coil design and use of poloidal field shaping can reduce residual vacuum magnetic islands and increase the effective plasma size. Figure 4 shows the improvement that can be obtained in the calculated vacuum magnetic surfaces for the Uragan-2M device by modifying the amplitude β of the $\sin 2\theta$ modulation of the helical winding trajectory given by $\phi = (\theta - \alpha \sin \theta - \beta \sin 2\theta)/2$, where ϕ and θ are the toroidal and poloidal angles, respectively (Bykov *et al.*, 1989). Maximization of the plasma size by optimizing the helical winding trajectory has also been done in the Compact Torsatron study (Carreras *et al.*, 1987) and in the design of the small Compact Auburn Torsatron (Gandy *et al.*, 1990) by using the Cary-Hanson technique (Hanson and Cary, 1984). Another, experimentally more flexible and dynamic method of flux surface restoration is via optimization of the currents in the poloidal field coil sets (Carreras *et al.*, 1987; Besedin *et al.*, 1990).

Field errors can essentially be avoided by constructing coils with many turns, as on CHS and on future large experiments with superconducting coils. Field mapping measurements on CHS in early 1990 showed no change from the measurements at 0.1 T in June 1988: a small (≈ 1 -cm) island at the $\iota = 1/2$ surface whose size scaled as $B^{-1/2}$ (a constant field perturbation) and a larger island at $\iota = 1$ with a clear boundary and no signs of ergodization (Okamura, 1990).

ORNL-DWG 90-2903 FED

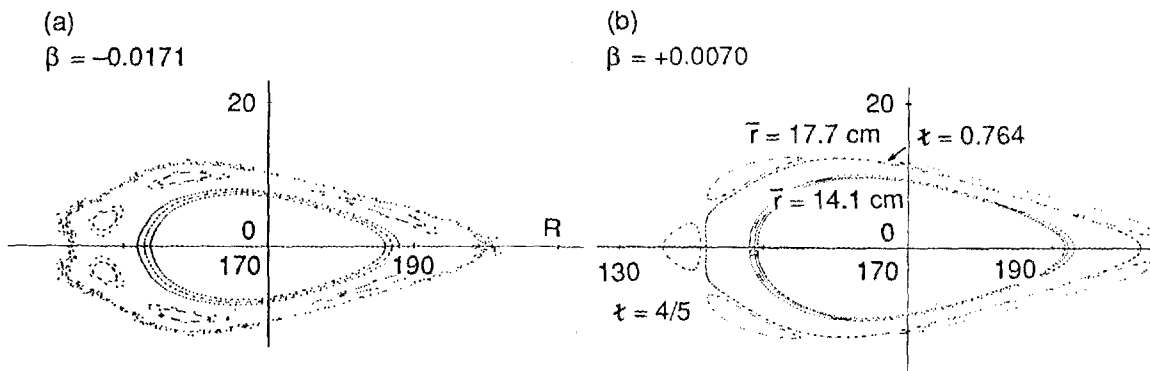


Fig. 4. Calculated magnetic flux surfaces for Uragan-2M for two different values of the $\sin 2\theta$ modulation of the helical winding pitch: (a) $\beta = -0.0171$ (design value) and (b) $\beta = 0.0070$.

Resonant field perturbations can be deliberately added to create magnetic islands and to study their effects. On Heliotron DR (Morimoto *et al.*, 1990), an externally applied $m = n = 1$ perturbation with $B_{1,1}/B \sim 3 \times 10^{-4}$ produced a large island at $\epsilon = 1$ ($r/\bar{a} \sim 0.5$) and a significant deterioration of plasma confinement. However, a perturbing field that produced a set of many islands with high poloidal (m) and toroidal (n) mode numbers ($m = 5, 4, 3$; $n = 5, 6, 7, 8, 9, 10$), extending from $r/a \simeq 0.5$ to $\simeq 1$, that should overlap did not lead to confinement deterioration; in this case, large magnetic fluctuations due to plasma turbulence may have dominated the plasma behavior. An added $m = n = 1$ field error on Heliotron E produced a 10-cm-wide band of poor flux surfaces near $\epsilon = 1$, as expected from calculations. Error field coils will be installed on ATF in early 1991 to simulate the earlier field errors for study of their effect on confinement and for more controlled access to the second stability region at lower beta as a result of the reduced plasma size, as discussed in Sect. 6.2.

4.2 Bootstrap Currents

An important consequence of finite plasma pressure is a net bootstrap current, which can provide part of the toroidal plasma current that is needed in tokamaks but could compromise zero-current operation in stellarators and distort $\epsilon(r)$ in an unfavorable manner for stability and transport.

Neoclassical calculations of the bootstrap current have been confirmed by experiments in ATF (Murakami *et al.*, 1990b). Figure 5 shows the agreement of the neoclassical predictions for the bootstrap current and the measured plasma current as the quadrupole moment of the poloidal field is varied for 0.3-MW ECH plasmas.

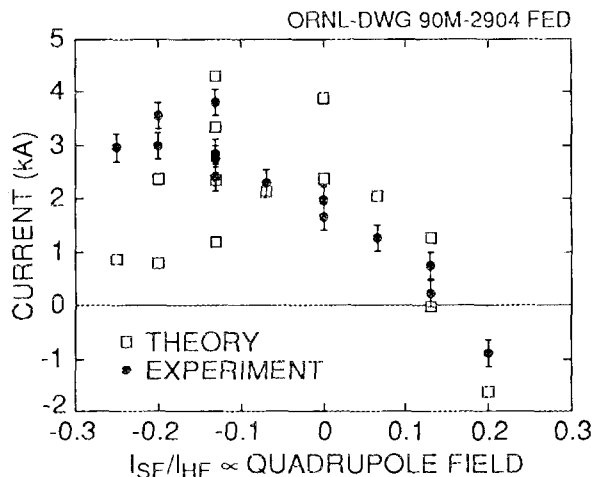


Fig. 5. Measured toroidal plasma currents and neoclassical predictions of the bootstrap current as functions of the ratio of the shaping field current I_{SF} (proportional to the quadrupole moment of the poloidal field) to the helical field current I_{HF} in ATF.

The experimental error bars correspond to measurement uncertainties and to shot-to-shot variations in the net plasma current. The measured current is not an Ohmic current because the loop voltage is < 0.003 V, nor is it due to ECH current drive because the ECH launch is perpendicular to B , the current reverses when the helical field is reversed, and the current increases with \bar{n}_e instead of $1/\bar{n}_e$. Agreement is also obtained for experiments in which the vacuum magnetic axis shift is varied. Both experiments show that the bootstrap current can be reduced to zero or even reversed without current drive and that the bootstrap current is approximately neoclassical in nature, even though the particle and heat transport are anomalous by much larger factors. These experiments increase confidence in use of the neoclassical bootstrap current formulation in optimizing stellarator configurations.

5. TRAPPED-PARTICLE LOSSES

One aspect of configuration optimization is improvement of the confinement of helically trapped particles, which have a loss region for small v_{\parallel}/v (pitch angle $\sim 90^\circ$). Figure 6 shows the loss region (on the large- R side) calculated for LHD (Iiyoshi *et al.*, 1990). Small inward shifts (10–15 cm in 400 cm) of the vacuum magnetic axis would dramatically reduce the size of the loss region and consequently

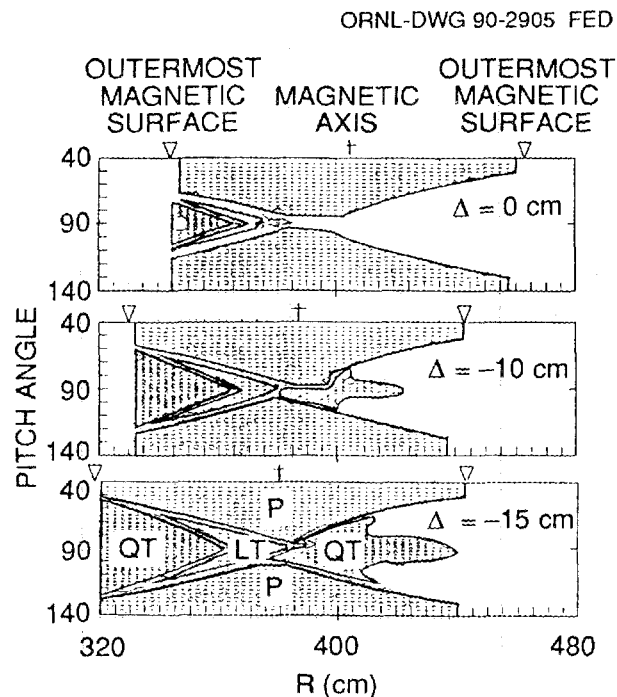


Fig. 6. Classes of confined particles (shaded areas) and the loss region (unshaded area) at a toroidal angle of 18° for different axis shifts Δ calculated for LHD. Here P = passing particles, LT = locally trapped particles, and QT = quasi-trapped particles.

the fraction of the helically trapped particles that are lost, as illustrated in Fig. 7. This loss of energetic particles may limit the use of heating schemes that produce energetic particles with small v_{\parallel}/v (perpendicular NBI and some forms of ICRF heating) and may cause a significant loss of alpha particles in a reactor [although recent studies (Painter and Lyon, 1990) indicate that such losses are acceptable and provide an inherent, effective helium ash removal mechanism].

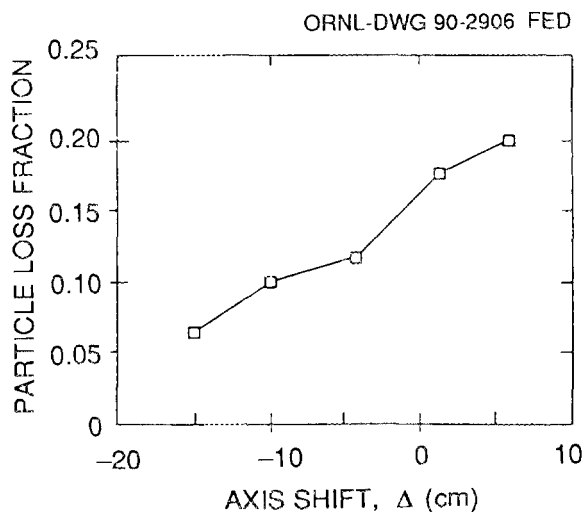


Fig. 7. Fraction of particles lost in LHD for different shifts of the vacuum magnetic axis.

The extent and effects of the near-perpendicular loss region are being studied in a complementary fashion in ATF and CHS. ATF has fixed tangential NBI and a two-dimensional (2-D) scanning neutral particle analyzer (NPA) that can scan from tangential in one direction through perpendicular to tangential in the opposite direction, whereas CHS has a scanning NPA and a 1.2-MW neutral beam line that can be moved from tangential to perpendicular. A third neutral beam line is being installed on ATF for perpendicular injection, and this should allow better studies of the energetic particle loss region at low v_{\parallel}/v . Studies of ECH on L-2 (Andryukhina *et al.*, 1990) indicate another effect: poorly confined fast trapped electrons localized in the region of the ECH launch can absorb a significant fraction of the input power while contributing little to the plasma stored energy.

The expected improvement in energetic orbit confinement (reduced loss region) for inward shifts ($\Delta < 0$) of the magnetic axis is confirmed in Heliotron E by the dependence on the axis shift of (1) the measured decay time of the perpendicularly injected beam ions following beam turnoff and (2) the loss time needed for good agreement between the measured time-dependent neutral particle flux and that calculated from the Fokker-Planck equation, as shown in Fig. 8 (Sano and Heliotron E Group, 1990). This is further evidence that energetic ions behave classically in stellarators.

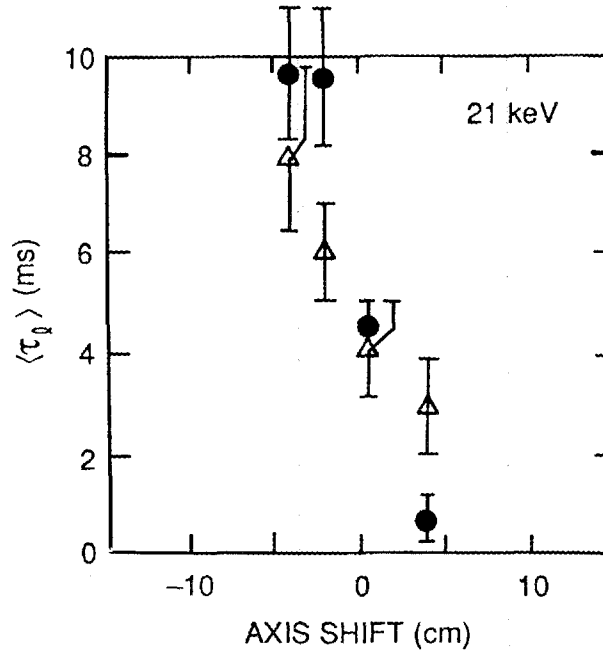


Fig. 8. Effective confinement time $\langle \tau_l \rangle$ for fast ions in Heliotron E at the NBI energy (21 keV) from the decay time after beam turnoff (solid circles) and from the shape of the steady-state energy spectrum (open triangles).

The best plasma performance in Heliotron E is found at $\Delta = -2$ cm, where the orbit deviation from a flux surface is a minimum. Figure 9 shows the results for an NBI-heated plasma (Sano and Heliotron E group, 1990). Small inward shifts of the vacuum magnetic axis also give the maximum values of the stored energy on ATF and CHS. However, shifting the vacuum magnetic axis inward changes a number of other configuration characteristics on Heliotron E, producing a larger magnetic hill, reduced effective helical ripple, a decrease in $\tau(0)$, and an increase in shear that peaks at $\Delta = -2$ cm, so factors other than improved orbit confinement may contribute to the improved performance.

Loss of helically trapped particles, and related ripple-induced transport, can be reduced by poloidal field shaping and radial electric fields. Calculations (Lyon *et al.*, 1990c) show that increasing the central transform in ATF can essentially eliminate the loss of energetic helically trapped particles, similar to the effect of an inward shift of the magnetic axis. However, both techniques lead to a higher bootstrap current and to less favorable MHD stability properties. On the other hand, radial electric fields should improve confinement of helically trapped particles and reduce neoclassical ripple-induced transport through $\vec{E} \times \vec{B}$ poloidal orbit rotation without a deleterious effect on stability. Taking advantage of electric field effects, which probably also play a role in the favorable transition from L-mode to H-mode in

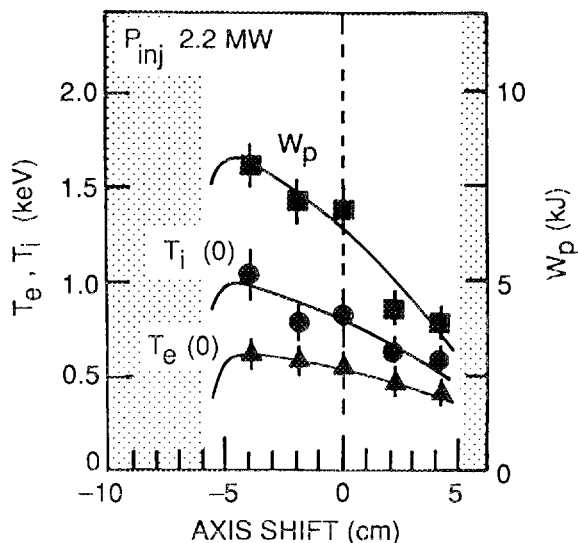


Fig. 9. Dependence on vacuum axis shift Δ of the central electron (T_e) and ion (T_i) temperatures and the plasma stored energy (W_p) for an NBI-heated plasma in Heliotron E.

tokamaks (Itoh and Itoh, 1988; Shaing *et al.*, 1990), is an important factor in stellarator optimization and is critical to the reactor extrapolation of low-aspect-ratio stellarators (Painter and Lyon, 1990).

External configuration control is a useful tool in studying the effects of trapped particles. For example, the dissipative trapped-electron mode can be studied more easily in stellarators than in tokamaks because of the configuration flexibility, the shorter connection length (lower effective collisionality), the toroidal localization of certain modes in the helical ripple, and the resulting larger radial extent of these modes in stellarators (Carreras *et al.*, 1990). In ATF, the driving term (the trapped-electron fraction) and the stabilizing term (the shear) can be varied from a stable configuration [no trapped particles confined and $\epsilon(0) \simeq 0$, hence large shear] to an unstable configuration [all trapped particles confined and $\epsilon = 0.36$ – 0.4 for $r/a = 0$ – 0.6 , hence a large central region with low shear] by changing the quadrupole component of the poloidal field.

6. FINITE-BETA BEHAVIOR

6.1 Maximum Beta Values

With the limited heating power available to date, MHD behavior and beta limits are best studied at lower magnetic field. Values of $\langle\beta\rangle = 1.5\%$ have been obtained recently with NBI on ATF at $B_0 = 0.63$ T and on CHS at $B_0 = 0.45$ – 0.49 T. Figure 10 shows the variation of $\langle\beta\rangle$ with shift of the magnetic axis for CHS

plasmas obtained with 1-MW tangential NBI (Yamada, 1990). The stored energy, from which $\langle\beta\rangle$ is calculated, is obtained from a diamagnetic loop measurement (parallel beam pressure not included). The best performance is obtained when the magnetic axis is located at 92 cm, 3 cm inside the axis position where the on-axis magnetic ripple vanishes. The $\langle\beta\rangle$ values obtained are still below the calculated limit for low- m ideal interchange modes. The magnetic fluctuations shown in Fig. 10, identified as low- m ($m = 1, 2, 3$) coherent modes, increase with inward magnetic axis shift (stronger magnetic hill); however, they do not seem to affect the beta achieved.

ORNL-DWG 90-2909 FED

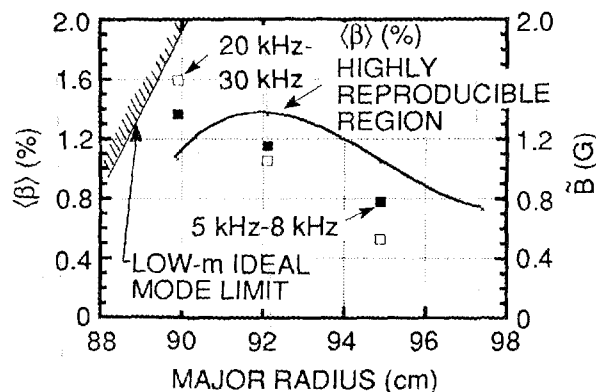


Fig. 10. Variation of the volume-average beta (curve) and typical magnetic fluctuation levels \tilde{B} in the frequency intervals 5–8 kHz (solid squares) and 20–30 kHz (open squares) for different positions (shifts) of the vacuum magnetic axis in CHS.

6.2 Second Stability Behavior

Beta self-stabilization occurs when the depth and radial extent of the magnetic well increase rapidly enough with increasing beta to offset the destabilizing effect of the increasing plasma pressure. Evidence for this behavior has been obtained in ATF (Harris *et al.*, 1989). Figure 11(a) shows that coherent $n = 1$ poloidal magnetic fluctuations (\tilde{B}_θ) are observed to first increase with beta and then decrease at higher values, even though the instability should be moving closer to the array of magnetic loops as beta increases. The same behavior is seen during the time evolution of a single discharge. On-axis beta values [$\beta(0) \leq 3\%$] are well above the theoretical value [$\beta(0) \simeq 1.3\%$ for ideal modes] for transition to the second stability regime for the peaked pressure profiles obtained in this earlier phase of ATF operation.

Beta self-stabilization is predicted to affect the stability of resistive pressure-gradient-driven modes as well as ideal MHD modes (Carreras, 1988). Multiple-helicity calculations of the nonlinear saturated amplitude of resistive modes (ballooning in the core and interchange near the edge) give $m = 2$, $n = 1$ and $m = 3$,

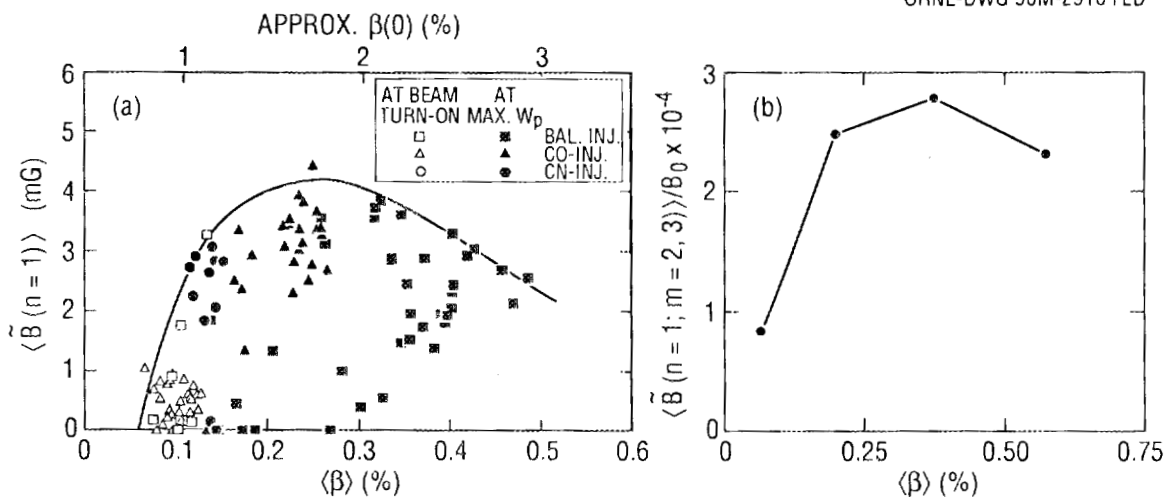


Fig. 11. Variation with beta of (a) the maximum amplitude of coherent $n = 1$ magnetic oscillations in ATF and (b) the saturated levels of the ($m = 2$, $n = 1$) and ($m = 3$, $n = 1$) magnetic fluctuations from theory.

$n = 1$ for the dominant components, as in the experiment, although linear theory predicts these modes to have lower growth rates than other modes (Charlton *et al.*, 1990); the beta dependence is the same as in the experiment [Fig. 11(b)].

Experimental broadening of the pressure profile with increasing beta, in much the same way that the calculated volume of the magnetic well increases (shown in Fig. 12; Harris *et al.*, 1989), and theoretical calculations of the saturated pressure profiles that are less turbulent above the transition to second stability than below

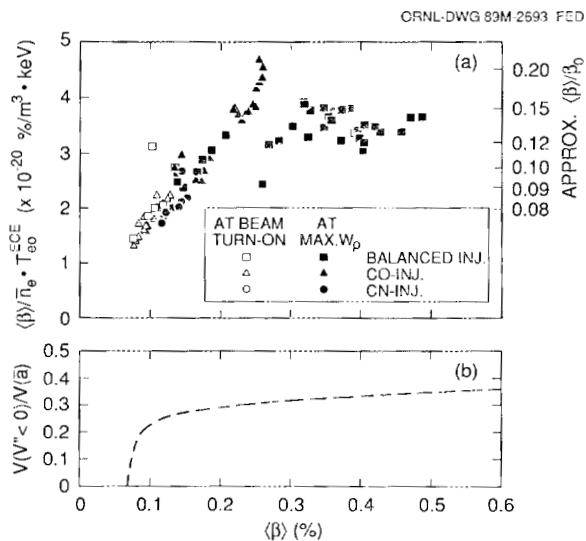


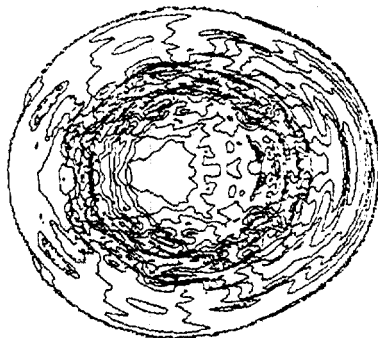
Fig. 12. (a) Broadening of the pressure profile in ATF with $\langle \beta \rangle$. (b) Calculated fraction of the plasma volume that has a magnetic well versus $\langle \beta \rangle$.

it (shown in Fig. 13; Charlton *et al.*, 1990) confirm that the beta self-stabilization process is occurring in ATF and that the plasma is following the path of ideal MHD marginal stability into the second stability regime.

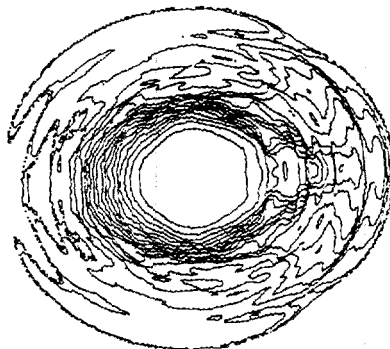
The achievement of second stability operation in ATF has several consequences: (1) it confirms the design basis for the set of beta self-stabilized stellarators with significant shear that are emphasized in this review; (2) it gives confidence in the predictions of higher beta in stellarators (and in tokamaks); (3) it suggests that the stability of nonideal curvature-driven or curvature-coupled modes that can be responsible for anomalous transport (such as the neoclassical extension of resistive interchange modes, trapped-electron modes, and η_i modes) could be improved; and (4) it provides an experimental method for separating instabilities that are coupled with curvature from those that are not.

ORNL-DWG 90-2911 FED

(a) $\beta_0 = 0.8\%$



(b) $\beta_0 = 2.3\%$



R →

Fig. 13. Perturbed pressure profiles in ATF calculated from the saturated nonlinear amplitude of a resistive mode for $\beta(0)$ (a) below and (b) above the transition to second stability for ideal MHD modes.

Optimization of both confinement and stability may require field shaping in addition to a magnetic axis shift. The additional configuration flexibility may be obtained through poloidal field (quadrupole) shaping, as on ATF and LHD, or through an added toroidal field, as on Heliotron E. Figure 14(a) shows the variation of W_p and τ_E with $\alpha^* = B_t/B_h$ for a Heliotron E configuration shifted in by 2 cm ($\Delta = -2$ cm). Here B_t is the added toroidal field and B_h is the toroidal field produced by the helical windings. The plasma was produced with 53.2-GHz ECH and heated by 2.2-MW NBI with $B_0 = 1.76$ T ($\alpha^* < 0$) or 1.9 T ($\alpha^* > 0$). The best performance ($W_p = 16$ kJ, $\tau_E = 9$ ms) is obtained at $\alpha^* = 0.05$ – 0.1 (Kondo *et al.*, 1990). The peaks in W_p and τ_E in Fig. 14(a) for $0.05 \lesssim \alpha^* \lesssim 0.1$ correspond to magnetic-well stabilization of internal disruptions ($m = 2$, $n = 1$ mode at the $r = 1/2$ surface), as indicated in Fig. 14(b) (Obiki *et al.*, 1990b). Low-frequency (8- to 20-kHz) $m/n = 1/1$, $2/1$, and $2/3$ fluctuations, thought to be resistive interchange modes, and drift-wave-type density fluctuations below 100 kHz were also stabilized for $0.05 \lesssim \alpha^* \lesssim 0.1$.

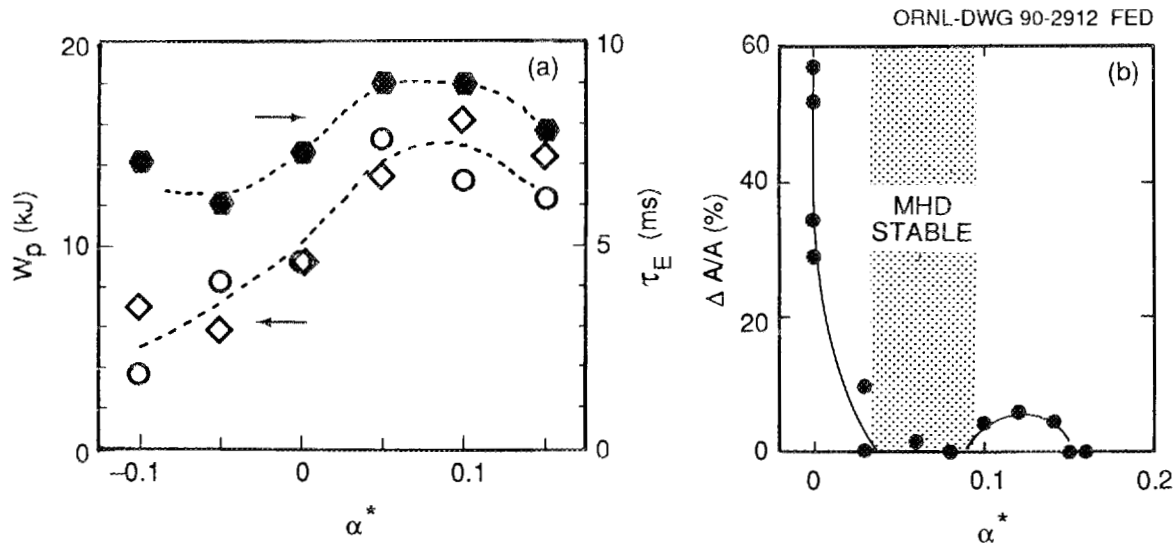


Fig. 14. Dependence on added toroidal field ($\alpha^* = B_t/B_h$) of (a) plasma stored energy W_p from diamagnetic (open circles) and kinetic (open diamonds) measurements and global τ_E (solid hexagons) and (b) the change in the soft X-ray intensity at the sawtooth crash for NBI-heated plasmas in Heliotron E.

7. GLOBAL CONFINEMENT SCALING

Understanding the scaling of energy confinement and the processes responsible is even more important in stellarators than it is in tokamaks because of the larger configuration space covered by stellarators and the smaller number of experiments. Figure 15 shows an empirical confinement scaling (Sudo *et al.*, 1990b), derived

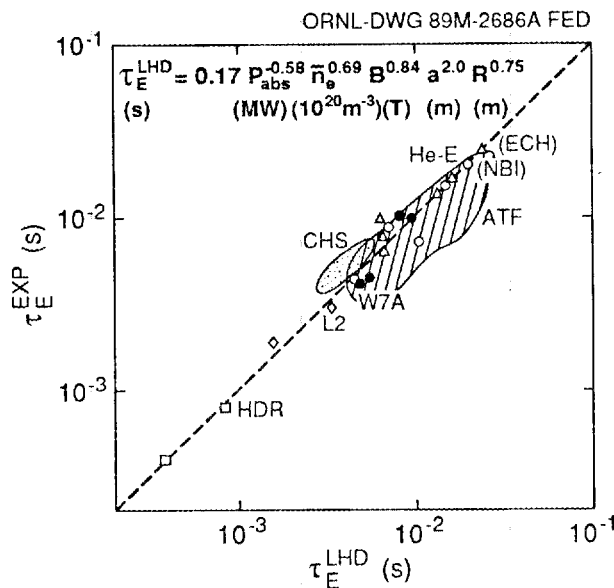


Fig. 15. The LHD scaling relation for global energy confinement time τ_E versus experimental values from a number of stellarator experiments.

mainly from Heliotron E data, that has been used in the LHD design studies. The LHD empirical scaling relation for stellarators, given by

$$\tau_E^{LHD}(\text{s}) = 0.17 P(\text{MW})^{-0.58} \bar{n}_e (10^{20} \text{ m}^{-3})^{0.69} B_0(\text{T})^{0.84} \bar{a}(\text{m})^2 R_0(\text{m})^{0.75},$$

fits data from a wide range of stellarators. Recent results from CHS, ATF, and Heliotron E confirm this general trend, although some deviations have been noted. On CHS, higher values are obtained at lower densities and with inward axis shifts (Matsuoka *et al.*, 1990), and on Heliotron E, a scaling faster than \bar{a}^2 is noted in scans of the vacuum axis shift (Sano and Heliotron E Group, 1990).

The improvement in τ_E^{LHD} with density and magnetic field offsets the degradation with power. If the LHD τ_E scaling is combined with a maximum density scaling proposed by Sudo *et al.*, (1990b), $(\bar{n}_e)_{\text{max}} = 0.25(PB_0/R_0\bar{a}^2)^{1/2}$, then τ_E^{LHD} is proportional to $P^{-0.24} B_0^{1.2} \bar{a}^{1.3} R_0^{0.4}$ with a weak negative dependence on power and a stronger positive dependence on magnetic field and plasma radius.

The LHD τ_E scaling is remarkably similar to a gyro-reduced Bohm scaling estimate for τ_E (Goldston *et al.*, 1989) for tokamaks based on the properties of saturated drift-wave turbulence (Perkins, 1984) and a simple scaling argument:

$$\tau_E^{\text{dw}}(\text{s}) = 10^{-9} P(\text{W})^{-3/5} \bar{n}_e(\text{m}^{-3})^{3/5} B_0(\text{T})^{4/5} \bar{a}(\text{m})^{12/5} R_0(\text{m})^{3/5} \kappa A_i^{-1/5},$$

where κ is the plasma elongation and A_i the ion mass. Except for the A_i and I_p dependences, this scaling is a good fit to the tokamak L-mode data base, and it may be a better fit to the ATF data than the LHD scaling. All of the individual

parametric dependences, including A_i , are consistent with those observed in stellarators. Trapped-particle drift-wave-type instabilities could be important in both stellarators and tokamaks. A contradictory observation is that the heat diffusivity χ generally increases with minor radius r in experiments rather than decreases, as theory would suggest. More development of the theory and systematic experiments are needed to determine whether a more fundamental process that is common to all toroidal experiments is responsible for anomalous transport, either directly (e.g. convective transport) or indirectly (through determining the saturated level of turbulence arising from different instabilities).

As in the case of tokamak L-mode scaling, the LHD and gyro-reduced Bohm scalings are a factor of 2-3 below that desired for an attractive reactor. The similarity of the confinement scaling and of the edge properties, including fluctuations, in tokamaks and stellarators combined with the higher degree of external control in stellarators suggests that H-mode-like improvements in confinement should be possible. In addition to the H-mode techniques developed on tokamaks, techniques that should be tried include (1) application of electric fields (through biased limiters, perpendicular NBI or electron beam injection, preferential heating-induced loss of ions or electrons, etc.) to reduce both turbulent fluctuations (Shaing *et al.*, 1990) and the loss of helically trapped particles, which are a source of free energy for instabilities and of potentially large neoclassical losses, and (2) operation in the second stability region, where turbulent fluctuations (and associated transport) may be reduced.

Particle confinement scaling studies are at a more primitive level than energy confinement scaling studies. Figure 16 shows the scaling obtained on Heliotron E

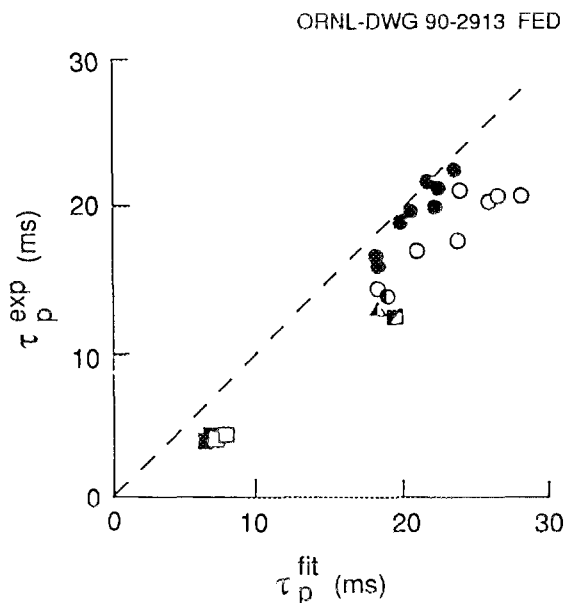


Fig. 16. Particle confinement times derived from H_α laser fluorescence measurements for different values of magnetic field B , added toroidal field α^* , and vacuum magnetic axis shift Δ versus an earlier fit for the standard ($\alpha^* = 0$, $\Delta = 0$) configuration in Heliotron E.

(Uchino *et al.*, 1988), where $\tau_p^{\text{fit}}(\text{s}) = 0.01P(\text{MW})^{-0.42}B(\text{T})^{1.23}$. The dependence on power and field is reminiscent of the LHD τ_E scaling, but the dependence on density and other parameters is not well defined yet.

8. LOCAL TRANSPORT STUDIES

Understanding of the confinement scaling and of the mechanisms responsible for it must come from detailed radial power balances and determination of the local heat diffusivities and their changes with plasma and configuration parameters rather than from global confinement studies. Examples from CHS (Iguchi *et al.*, 1990) are chosen to illustrate the observations and uncertainties.

Figure 17 shows the electron density and temperature profiles obtained for a sequence of discharges in the $1/\nu$ regime (stellarator collisionality $\nu^* \leq 1$) on CHS with 28-GHz and 53-GHz ECH. The shapes of the electron density and temperature profiles are the same at higher collisionality (in the plateau regime, $\nu^* \sim 5$) with only 28-GHz ECH, where the density is twice as high and the electron temperature half as high as in Fig. 17. Broader profiles are obtained with NBI-heated plasmas in the plateau regime. Figure 18 shows the electron density and temperature profiles obtained with 0.9-MW, 40-kV, coinjected NBI at $B_0 = 1.5$ T. The ion temperature profile obtained from charge-exchange recombination spectroscopy is broader than the electron temperature profile. In general, the density profiles in CHS and ATF (and also in Wendelstein VII-AS) are flat or even hollow, although peaked $n_e(r)$ can be obtained with pellet injection. Heliotron E routinely obtains more peaked profiles than in ATF or CHS, but the reason for this is not yet understood.

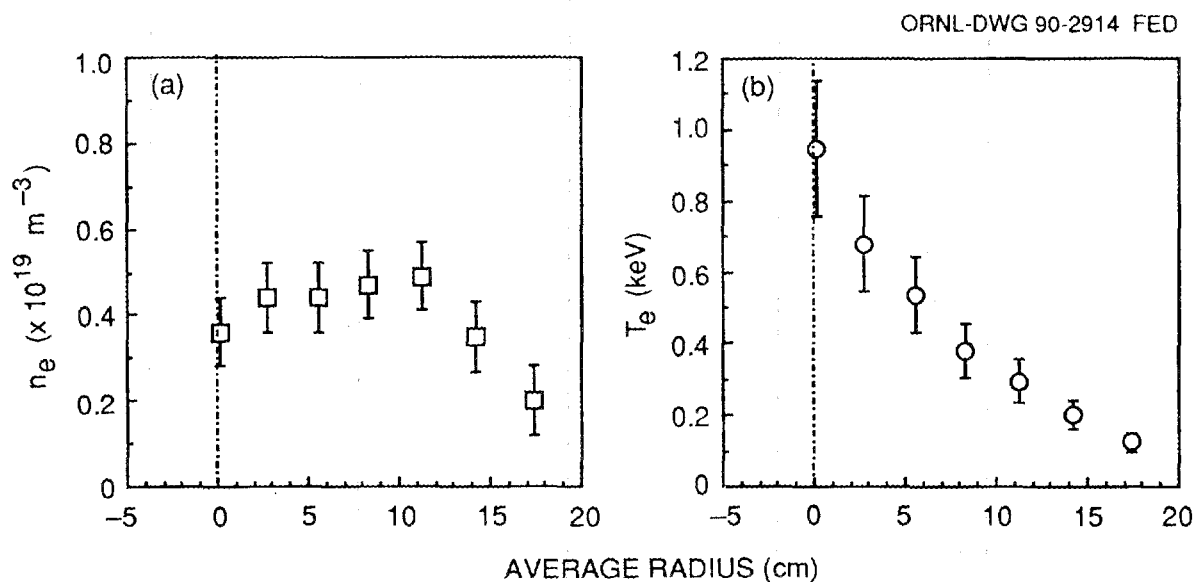


Fig. 17. Radial profiles of electron density and temperature for an ECH plasma (90 kW of 28-GHz power, 150 kW of 53-GHz power, $B = 0.9$ T, at $t = 30$ ms) in the $1/\nu$ regime in CHS.

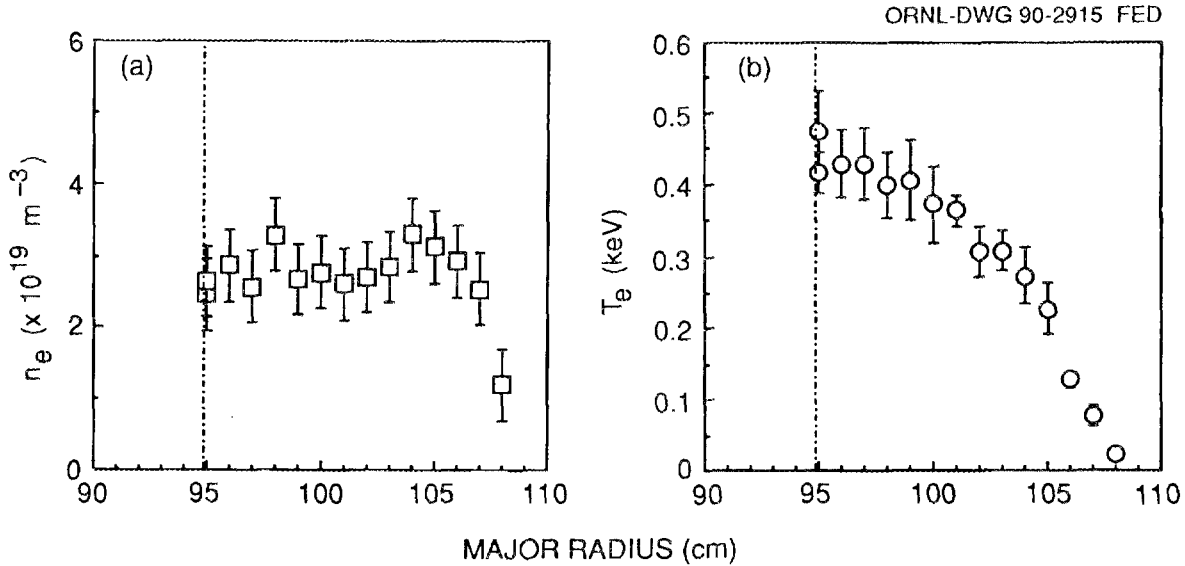


Fig. 18. Radial profiles of electron density and temperature for an NBI-heated plasma (900 kW, $B = 1.5$ T, at $t = 80$ ms) in the plateau regime in CHS.

The power deposition profile needed for determining the electron thermal diffusivity χ_e in CHS is calculated by assuming that the ECH power absorbed on a magnetic surface is proportional to the volume of the resonance layer at low density (low single-pass absorption) for 28-GHz ECH and that the heating efficiency is proportional to $n_e T_e$ (fairly peaked at the center) for second-harmonic 53-GHz ECH, which is consistent with measurements of the electron temperature decay after ECH turnoff. The power deposition profile for the NBI case is obtained from calculation of the birth profile of the fast ions. A significant broadening of the power deposition profile that is due to a $\simeq 6$ -cm outward orbit shift of the beam ions from the magnetic axis is not yet included in the analysis.

Figure 19 shows the inferred $\chi_e(r)$ for this sequence of CHS discharges: ECH at low ($1/\nu$) collisionality [$n_e(r)$ and $T_e(r)$ shown in Fig. 17], ECH at higher (plateau) collisionality, and NBI at higher (plateau) collisionality [$n_e(r)$ and $T_e(r)$ shown in Fig. 18]. In Fig. 19(a), the value of χ_e at $r/a = 1/2$ is $\simeq 7 \text{ m}^2/\text{s}$, about four times larger than that from a single-helicity neoclassical calculation of ripple-induced diffusion. At higher collisionality with ECH [Fig. 19(b)], χ_e is lower but the anomaly is higher ($\simeq 10$ at $r/a = 1/2$). The dashed portion of the electron heat diffusivity in Fig. 19c is due to the uncertainty in the NBI power deposition in the plasma core. The value of χ_e at $r/a = 2/3$ is $\simeq 3 \text{ m}^2/\text{s}$, about 20 times the neoclassical value. The anomaly factor is higher than with ECH and increases with density. In all cases, χ_e is anomalous and more constant than the neoclassical value, suggesting that another mechanism is responsible. Lack of an accurate Z_{eff} measurement makes estimation of the power deposition for the ions more uncertain than for the electrons. Assuming $Z_{\text{eff}} = 2$ gives a χ_i of the same order as χ_e and a smaller anomaly factor than for the electrons.

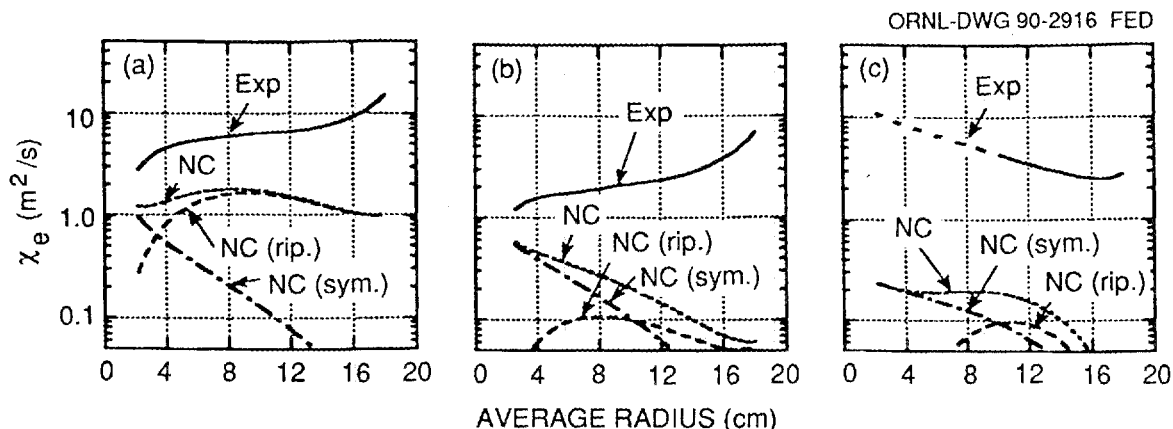


Fig. 19. Radial profiles of electron thermal diffusivity in CHS for (a) an ECH plasma in the $1/\nu$ (ripple transport) regime, (b) an ECH plasma in the plateau regime, and (c) an NBI plasma in the plateau regime. Exp: inferred from measurements. NC: neoclassical χ_e . NC (sym): axisymmetric (tokamak) contribution to total neoclassical χ_e . NC (rip): ripple-induced contribution to neoclassical χ_e .

The effect of the ambipolar radial electric field on transport needs to be studied. Experiments in Wendelstein VII-A indicate large radial electric fields ($E_r \sim 1$ kV/cm) with perpendicular NBI (into the loss region), and calculations indicate that χ_i is reduced from the plateau value to close to Pfirsch-Schlüter values (Maassberg *et al.*, 1985). Experiments in Heliotron E show a reversal of electric field at lower collisionality, as would be expected neoclassically. Recent Doppler-shift measurements of poloidal rotation velocities in CHS indicate a negative electric field $|E_r| > 100$ V/cm at the plasma edge that is larger than that expected neoclassically (Ida, 1990).

A 2-D heavy ion beam probe (HIBP) has been installed on ATF for mapping of the electric field over most of the plasma cross section. The 2-D measurements are important because probe measurements of the electric potential surfaces in IMS indicate that magnetic surfaces are not equipotential surfaces, so $\vec{E} \times \vec{B}$ convective transport is important in the hollow-density ECH plasmas in that experiment (Talmadge *et al.*, 1989). The HIBP will also allow measurement and correlation of density and potential fluctuations (and hence of the associated transport) deep in the plasma, as well as providing information on electric fields for assessment of energetic orbit losses, neoclassical ripple-induced transport, reduction of anomalous transport, and convective transport.

9. FLUCTUATION STUDIES

Turbulent fluctuation-induced transport is being examined as a candidate for anomalous transport in stellarators (and in tokamaks). The most developed techniques involve measurements of density fluctuations, but information is also being obtained from potential fluctuations and from magnetic fluctuations. Figure 20

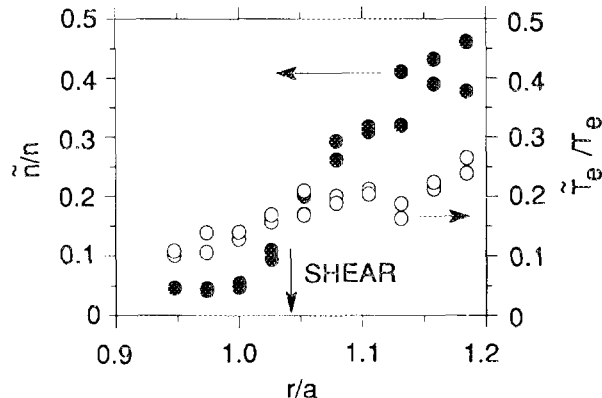


Fig. 20. Radial profiles of normalized density fluctuations (\tilde{n}_e/n_e , solid circles) and of an upper bound to normalized electron temperature fluctuations (\tilde{T}_e/T_e , open circles) near the plasma edge, obtained with a fast reciprocating Langmuir probe array in ATF.

shows the normalized density and electron temperature fluctuation levels in ATF near the plasma edge (Hidalgo *et al.*, 1990). The \tilde{T}_e/T_e data points indicate an upper bound on the relative electron temperature fluctuation level. The \tilde{n}_e/n_e and \tilde{T}_e/T_e levels are not equal and have different radial dependences. Both increase with radius; \tilde{n}_e/n_e is larger outside the plasma, and \tilde{T}_e/T_e is larger inside and has a significant level. The crossing point for \tilde{n}_e/n_e and \tilde{T}_e/T_e occurs at the velocity shear layer (indicated by the vertical arrow), where the poloidal fluctuating phase velocity reverses from propagation in the electron diamagnetic drift direction for $r/\bar{a} < 1$ to the ion diamagnetic direction for $r/\bar{a} > 1$ and where the poloidal correlation length of the fluctuations is sharply reduced. The particle flux inferred from these electrostatic fluctuations is consistent with the global particle balance estimated from H_α measurements if toroidal and poloidal symmetry is assumed. Similar edge behavior is observed on the TEXT tokamak and leads to similar conclusions. This suggests again that the underlying processes are similar despite the magnetic configuration differences.

Figure 21 shows density fluctuation spectra measured deeper in an ECH plasma in ATF with a two-frequency microwave reflectometer. Peaks in the range from 10 to 80 kHz associated with rational magnetic surfaces in the gradient region at $\tau \geq 1/2$ are observed at $r/\bar{a} \simeq 0.85$ but not at $r/\bar{a} \simeq 0.83$ or 0.9. The sharp radial localization allows study of fluctuations on a particular magnetic surface. Injection of a small pellet into an ECH plasma will also be used in ATF as a diagnostic to perturb the transport and to localize the microwave reflectometer fluctuation measurement to the resulting gradient region. The radial correlation lengths are 1–2 cm inside ECH plasmas and < 0.5 cm at the edge of NBI plasmas. Density fluctuations deeper in an NBI plasma have been measured on Heliotron E (Sudo

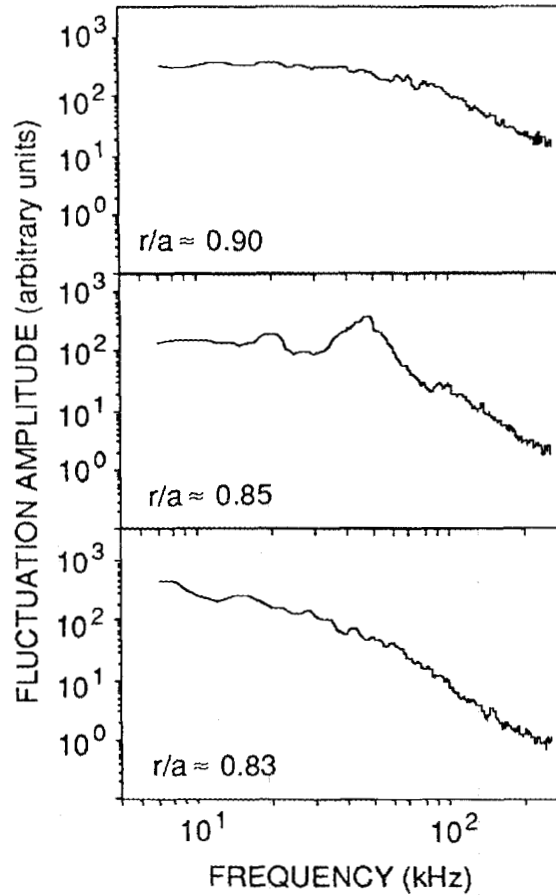


Fig. 21. Density fluctuation spectra obtained with a microwave reflectometer for an ECH plasma in ATF, showing the sharp radial dependence of the mode structure at 20 kHz and 40–60 kHz.

et al., 1990c) using Fraunhofer diffraction of a CO₂ laser beam. Fitting theoretical curves to the observed frequency spectra gives an ω - k relation that is consistent with that expected for drift waves.

Correlation has been observed between a change in the edge density fluctuation spectrum (a decrease of low-frequency components and an increase of high-frequency components) and a factor of 2–3 increase in W_p and τ_E in NBI plasmas in ATF (Anabitarte *et al.*, 1990). Correlation of density fluctuations with confinement properties has been observed in the L-2 stellarator (Batanov *et al.*, 1989). Measurements of the fluctuation spectra with a 2.5-mm collective scattering system showed that the central electron temperature decreased with increasing fluctuation amplitude and that above a certain level the energy confinement decreased (Fig. 22). A similar microwave scattering system is being developed by the L-2 group for measurements on ATF in a collaborative program.

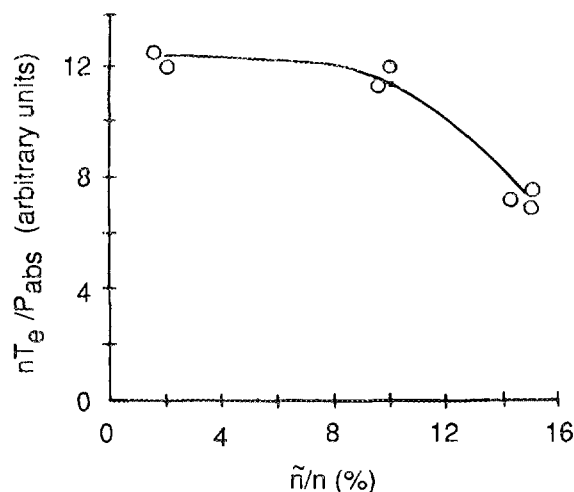


Fig. 22. Correlation of nT_e/P_{abs} (proportional to τ_E) with density fluctuation level for a 170-kW ECH discharge in L-2.

10. PARTICLE AND IMPURITY CONTROL

Because confinement improves with density, operation at higher density is preferred in the stellarators discussed here. Injection of multiple pellets into NBI plasmas has been used in Heliotron E (Sudo *et al.*, 1990a) to increase the density (as shown in Fig. 23) and to change the peaking of the density profile for transport studies. The slow decay of the density in Fig. 23 indicates a long particle confinement time ($\tau_p \gg \tau_E$).

Laser ablation of aluminum and scandium in ATF also indicates long impurity confinement times in NBI plasmas ($\tau_Z \gg \tau_E$). Agreement between the measured and modeled emission rates of various impurity lines in ATF gives estimated particle diffusivities that increase from $0.1 \text{ m}^2 \cdot \text{s}^{-1}$ at the center to $0.5 \text{ m}^2 \cdot \text{s}^{-1}$ at the edge in ECH plasmas and decrease from $0.5 \text{ m}^2 \cdot \text{s}^{-1}$ at the center to $0.05 \text{ m}^2 \cdot \text{s}^{-1}$ at the edge in NBI plasmas; the best comparison is obtained by assuming that there is no radial convective velocity (Horton *et al.*, 1990).

The long impurity confinement times can lead to impurity accumulation and subsequent radiative collapse, but this has not occurred in recent experiments in the stellarators discussed here. As discussed in Sect. 3, the pulse durations are now limited by the heating pulse length. On ATF, the fraction of the power radiated is typically $\lesssim 25\%$. Titanium gettering ($\approx 70\%$ coverage) has reduced the carbon and oxygen radiation to low levels and increased the metal radiation (Isler *et al.*, 1990).

The most important effect of titanium gettering is to reduce the hydrogen recycling from the wall. This allows tailoring of the gas puff and high-density operation. However, gettering and other wall pumping techniques cannot be used in future steady-state operation. Fortunately, these devices have a built-in helical divertor that can be used for steady-state removal of particles, impurities, and

ORNL-DWG 90-2920 FED

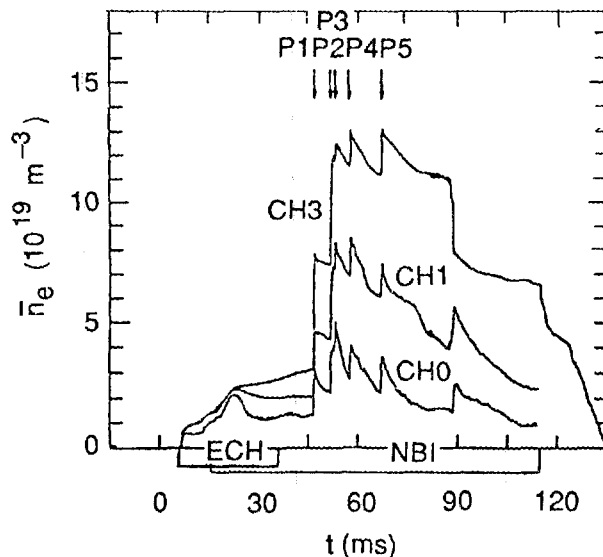


Fig. 23. Line-averaged density in Heliotron E with injection of hydrogen pellets into an NBI plasma. Signals for different vertical chords of the FIR interferometer array are shown. The arrows P1 to P5 indicate the times at which the pellets were injected.

power escaping from the plasma. Figure 24 shows the calculated diverted flux pattern in Heliotron E; the baffle plate indicated is part of a partial (one-fifth of the torus) helical divertor test. The neutral densities in the baffled (divertor module) and nonbaffled sections of the partial helical divertor were different and consistent with theoretical predictions, but the incomplete and unoptimized system did not affect the overall plasma parameters. Measurements on ATF (Mioduszewski *et al.*, 1989) indicate that the helical divertor stripes have a half-width of ≈ 2 cm and follow the calculated pattern. The divertor structure has also been measured on the Proto-Cleo stellarator (Anderson, 1989) at the University of Wisconsin. The plasma density along the helical divertor stripe is sharply peaked on the inboard (small- R) side. The escaping particle flux was localized near one polarity of the helical conductors.

11. CONCLUSIONS

The key optimization issues for stellarators with significant shear are being addressed at relevant parameters on complementary experiments. The main results from recent experiments indicate that:

- (1) The quality of vacuum magnetic surfaces can be controlled.
- (2) The bootstrap current is approximately neoclassical and can be controlled and used in configuration optimization studies.

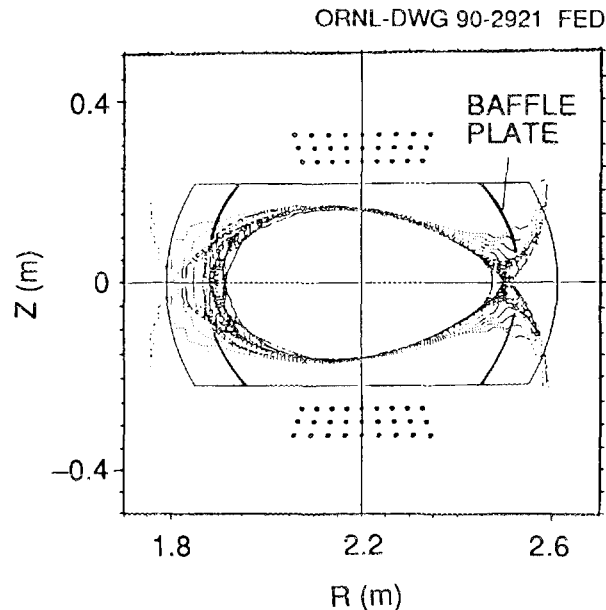


Fig. 24. Trajectory of magnetic field lines launched just outside the last closed flux surface in Heliotron E.

- (3) Both calculations and experiments show that the loss of helically trapped particles can be reduced.
- (4) The observation of second stability in ATF and other studies at moderate beta confirm the MHD basis for configuration optimization.
- (5) Confinement optimization favors a small (up to a few percent) inward shift of the magnetic axis; orbit confinement is improved and the finite-beta shift can maintain a magnetic well.
- (6) Confinement scaling is similar to that in tokamaks, but the positive density and field dependence offsets the degradation with increasing power.
- (7) Local transport studies indicate that the electron energy transport is anomalous.
- (8) Fluctuations are being studied as the source of the non-neoclassical losses, and some correlation with confinement has been observed.
- (9) Particle and impurity control is not a major issue at present, but helical divertors will be required for steady-state operation.

Stellarators with significant shear are maturing as a confinement concept. The key optimization issues are being addressed, as summarized above, with encouraging results that validate the optimization approach. There is now a focus on a common approach that leads to the next-generation LHD under design in Japan. The research is also relevant to tokamaks; similar confinement and plasma behavior are observed, and the external configuration control in stellarators is proving to be a useful toroidal research tool.

However, higher power is needed for more relevant physics and optimization studies. Heating powers of 1–2 MW are not sufficient for devices of the size of CHS

and ATF. Because the confinement improves with density, the best performance is obtained at high density where the ion temperature is low; more power is needed to increase T_i and T_e . More power is also needed to study optimization of confinement at higher $\langle\beta\rangle$, to demonstrate second stability (and resulting improved confinement) at higher $\langle\beta\rangle$, and to attain lower collisionality for studies of the bootstrap current and its control at larger currents.

Longer-pulse heating is also required to address optimization and control issues. Additional short-pulse heating is planned (0.5-MW, 106-GHz ECH on Heliotron E and ATF; 1-MW, 9- to 29-MHz ICRF on ATF; and an additional neutral beam line on ATF and CHS), but $\simeq 0.3$ s is too short to reach an equilibrium state in these experiments and to explore the issues of density and impurity control and handling high time-averaged power densities on the vacuum vessel walls and in the divertor that will be necessary for steady-state operation.

ACKNOWLEDGMENTS

Most of the material discussed in this review has been taken from papers presented at the 17th European Conference on Controlled Fusion and Plasma Physics in Amsterdam, June 25–29, 1990; from papers published in recent conference proceedings and journals; and from talks at recent meetings. The author thanks those who provided this material and those who granted permission for use of unpublished results. Special acknowledgements are due B. A. Carreras, J. H. Harris, R. C. Isler, M. Murakami, and the ATF group, Oak Ridge National Laboratory; D. T. Anderson, University of Wisconsin; K. Kondo, T. Obiki, and F. Sano, Kyoto University Plasma Physics Laboratory; L. M. Kovrizhnykh, General Physics Institute (Moscow); K. Matsuoka, National Institute for Fusion Science (Nagoya); O. S. Pavlichenko, Kharkov Institute of Physics and Technology; and H. Wobig, Max-Planck-Institut für Plasmaphysik (Garching). The author also acknowledges the encouragement and continued support of J. Sheffield of Oak Ridge National Laboratory.

REFERENCES

- Anabitarte, E. *et al.* (1990). Density fluctuation measurements on ATF using a two-frequency reflectometer. In: *Proc. 17th European Conf. on Controlled Fusion and Plasma Physics*, Amsterdam, Europhysics Conf. Abstracts, Vol. 14B, part IV, pp. 1492-1495.
- Anderson, D.T. (1989). Preliminary studies of the divertor structure in the Proto-CLEO stellarator. *Stellarator News*, No. 5, August.
- Andryukhina, Eh.D. *et al.* (1990). Efficiency of electron-cyclotron plasma heating in the L-2 stellarator. In: *Proc. 17th European Conf. on Controlled Fusion and Plasma Physics*, Amsterdam, Europhysics Conf. Abstracts, Vol. 14B, part II, pp. 463-466.
- Batanov, G.M. *et al.* (1989). Small-scale density fluctuations in Ohmic and ECR heated plasma in L-2 stellarator. In: *Proc. 16th European Conf. on Controlled Fusion and Plasma Physics*, Venice, Europhysics Conf. Abstracts, Vol. 13B, part II, pp. 663-666.
- Berezhnyi, V.L. *et al.* (1989). Behavior of impurities during RF heating in the Uragan-3 torsatron. In: *12th Int. Conf. on Plasma Physics and Controlled Nuclear Fusion Research*, Nice, 1988, IAEA, Vienna, Vol. 2, pp. 599-609.
- Berezhnyi, V.L. *et al.* (1990). The first experimental results on the Uragan-3M torsatron. Submitted to the 13th Int. Conf. on Plasma Physics and Controlled Nuclear Fusion Research, Washington.
- Besedin, N.T. *et al.* (1990). Physics of Uragan-2M. Submitted to the 13th Int. Conf. on Plasma Physics and Controlled Nuclear Fusion Research, Washington.
- Bykov, V.E. *et al.* (1989). On vacuum field properties of the Uragan-2M torsatron standard configuration. Report IPP 2/301, Max-Planck-Institut für Plasma-physik, Garching.
- Carreras, B.A. (1988). Anomalous transport in the second stability regime. *Comments Plasma Phys. Controlled Fusion* **12**, 35-44.
- Carreras, B.A. *et al.* (1987). Low-aspect-ratio torsatron configurations. *Nucl. Fusion* **28**, 1195.
- Carreras, B.A. *et al.* (1988). Progress in stellarator/heliotron research: 1981-1986. *Nucl. Fusion* **28**, 1613-1694.
- Carreras, B.A. *et al.* (1990). Dissipative trapped electron modes in $\ell = 2$ torsatrons. In: *Proc. 1st Int. Toki Conf. on Plasma Physics and Controlled Nuclear Fusion*, Toki, Report NIFS-PROC-3, National Institute for Fusion Science, Nagoya, pp. 118-121.
- Charlton, L.A. *et al.* (1990). Resistive MHD studies for ATF plasmas during operation in the second stability regime. In: *Proc. 1st Int. Toki Conf. on Plasma Physics and Controlled Nuclear Fusion*, Toki, Report NIFS-PROC-3, National Institute for Fusion Science, Nagoya, pp. 41-44.
- Colchin, R.J. *et al.* (1989). Correction of field errors in the ATF torsatron. In: *Proc. 16th European Conf. on Controlled Fusion and Plasma Physics*, Venice, Europhysics Conf. Abstracts, Vol. 13B, part II, pp. 615-618.

- Gandy, R.F. *et al.* (1990). Design of the Compact Auburn Torsatron. In: *Proc. 1st Int. Toki Conf. on Plasma Physics and Controlled Nuclear Fusion*, Toki, Report NIFS-PROC-3, National Institute for Fusion Science, Nagoya, pp. 25–28.
- Goldston, R.J. *et al.* (1989). $\tilde{E} \times B/B^2$ vs. $v_{\parallel} \tilde{B}/B$ as the cause of transport in tokamaks. *Bull. Am. Phys. Soc.* **34**, 1964.
- Hanson, J.D. and Cary, J.R. (1984). Elimination of stochasticity in stellarators. *Phys. Fluids* **27**, 767.
- Harris, J.H. *et al.* (1989). Second stability in the ATF torsatron. *Phys. Rev. Lett.* **63**, 1249–1252.
- Hidalgo, C. *et al.* (1990). Edge turbulence studies in ATF. In: *Proc. 17th European Conf. on Controlled Fusion and Plasma Physics*, Amsterdam, Europhysics Conf. Abstracts, Vol. 14B, part III, pp. 1353–1356.
- Horton, L.D. *et al.* (1990). Impurity transport in ATF and the effect of controlled impurity injection. In: *Proc. 17th European Conf. on Controlled Fusion and Plasma Physics*, Amsterdam, Europhysics Conf. Abstracts, Vol. 14B, part II, pp. 447–450.
- Ida, K. (1990). Toroidal and poloidal rotation of CHS plasma. Presented at the IEA Workshop on Stellarators, July 2–6, 1990, Garching, FRG.
- Iguchi, H. *et al.* (1990). Transport study on ECH- and NBI-heated plasmas in the low-aspect-ratio helical system CHS. In: *Proc. 17th European Conf. on Controlled Fusion and Plasma Physics*, Amsterdam, Europhysics Conf. Abstracts, Vol. 14B, part II, pp. 451–454.
- Iiyoshi, A. *et al.* (1990). Design study for the Large Helical Device. *Fusion Technol.* **17**, 169–187.
- Isler, R.C. *et al.* (1990). Cleanup and improvement of operational performance of ATF by chromium and titanium gettering. In: *Proc. 17th European Conf. on Controlled Fusion and Plasma Physics*, Amsterdam, Europhysics Conf. Abstracts, Vol. 14B, part II, p. 455–458.
- Itoh, S.-I. and Itoh, K. (1988). Model of L- to H-mode transition in a tokamak. *Phys. Rev. Lett.* **60**, 2276–2279.
- Kondo, K. *et al.* (1990). Confinement and stability on Heliotron E plasma. In: *Proc. 17th European Conf. on Controlled Fusion and Plasma Physics*, Amsterdam, Europhysics Conf. Abstracts, Vol. 14B, part II, pp. 459–462.
- Kovrizhnykh, L.M. (1988). Heating and confinement of a stellarator plasma — a review of theory and experiments (1980–1985). *Plasma Phys. Controlled Fusion* **30**, 67–112.
- L-2 Team and ECR Group (1989). Review of experiments in the L-2 stellarator. *Plasma Phys. Controlled Fusion* **31**, 1705–1711.
- Lyon, J.F. *et al.* (1990a). Construction and initial operation of the Advanced Toroidal Facility. *Fusion Technol.* **17**, 33–50.
- Lyon, J.F. (1990b). Near-term directions in the world stellarator program. *Fusion Technol.* **17**, 19–32.
- Lyon, J.F. *et al.* (1990c). Advanced Toroidal Facility II studies. *Fusion Technol.* **17**, 188–205.

- Maassberg, H. *et al.* (1985). Ambipolar electric fields and transport. In: *Proc. 12th European Conf. on Controlled Fusion and Plasma Physics*, Budapest, Europhysics Conf. Abstracts, Vol. 9F, part I, pp. 389–392.
- Matsuoka, K. *et al.* (1990). Review of CHS experiment. In: *Proc. 1st Int. Conf. on Plasma Physics and Controlled Nuclear Fusion*, Toki, Report NIFS-PROC-3, National Institute for Fusion Science, Nagoya, pp. 93–96.
- Mioduszewski, P.K. *et al.* (1989). Edge plasma and divertor studies in the ATF torsatron. In: *Proc. 16th European Conf. on Controlled Fusion and Plasma Physics*, Venice, Europhysics Conf. Abstracts, Vol. 13B, part II, pp. 623–626.
- Morimoto, S. *et al.* (1989). Second harmonic electron cyclotron heating in low density and overdense plasmas in Heliotron DR. *Nucl. Fusion* **29**, 1697–1707.
- Morimoto, S. *et al.* (1990). Effects of perturbing helical fields on confinement of Heliotron DR plasma. In: *Proc. 1st Int. Toki Conf. on Plasma Physics and Controlled Nuclear Fusion*, Toki, Report NIFS-PROC-3, National Institute for Fusion Science, Nagoya, pp. 73–76.
- Murakami, M. *et al.* (1990a). Overview of recent results from the Advanced Toroidal Facility. In: *Proc. 1st Int. Toki Conf. on Plasma Physics and Controlled Nuclear Fusion*, Toki, Report NIFS-PROC-3, National Institute for Fusion Science, Nagoya, pp. 77–80.
- Murakami, M. *et al.* (1990b). Bootstrap current studies in the Advanced Toroidal Facility. In: *Proc. 17th European Conf. on Controlled Fusion and Plasma Physics*, Amsterdam, Europhysics Conf. Abstracts, Vol. 14B, part II, pp. 443–446.
- Nishimura, K. *et al.* (1990). Compact Helical System physics and engineering design. *Fusion Technol.* **17**, 86–100.
- Obiki, T. *et al.* (1990a). Recent Heliotron E physics study activities and engineering developments. *Fusion Technol.* **17**, 101–122.
- Obiki, T. *et al.* (1990b). Review of Heliotron E experiment. In: *Proc. 1st Toki Conf. on Plasma Physics and Controlled Nuclear Fusion*, Toki, Report NIFS-PROC-3, National Institute for Fusion Science, Nagoya, pp. 89–92.
- Okamura, S. (1990). Status of CHS. *Stellarator News* No. 9, May.
- Painter, S.L. and Lyon, J.F. (1990). Transport analysis of stellarator reactors. Submitted to *Nucl. Fusion*.
- Perkins, F.W. (1984). Confinement scaling in tokamaks: consequences of drift wave turbulence. In: *Proc. 4th Int. Symp. on Heating in Toroidal Plasmas*, Rome, Vol. II, pp. 977–988.
- Ringler, H. *et al.* (1990). Confinement studies on the Wendelstein VII-AS stellarator. *Plasma Phys. Controlled Fusion* **32** (this issue).
- Sano, F. and Heliotron E Group (1990). Confinement studies of Heliotron-E plasmas in magnetic surface variation experiments. In: *Proc. 1st Int. Toki Conf. on Plasma Physics and Controlled Nuclear Fusion*, Toki, Report NIFS-PROC-3, National Institute for Fusion Science, Nagoya, pp. 192–195.
- Sapper, J. and Renner, H. (1990). Stellarator Wendelstein VII-AS: physics and engineering design. *Fusion Technol.* **17**, 62–75.

- Shafranov, V.D. (1983). Magnetohydrodynamic theory of plasma equilibrium and stability in stellarators: survey of results. *Phys. Fluids* **26**, 357–364.
- Shaing, K.C. *et al.* (1990). Bifurcation of poloidal rotation and suppression of turbulent fluctuations: a model for the L-H transition in tokamaks. *Phys. Fluids B* **2**, 1492–1498.
- Shi, X.H. *et al.* (1988). Experimental investigation of different configurations in a flexible heliac. *Nucl. Fusion* **28**, 859–869.
- Shohet, J.L. and TSL Group (1990). Status of the torsatron/stellarator program. In: *Proc. 1st Int. Toki Conf. on Plasma Physics and Controlled Nuclear Fusion*, Toki, Report NIFS-PROC-3, National Institute for Fusion Science, Nagoya, pp. 85–88.
- Sudo, S. (1990). Recent activities on Heliotron E: magnetic surface mapping, movable ICRF antenna, and D₂O laser system. *Stellarator News* No. 7, January.
- Sudo, S. *et al.* (1990a). Profile measurements in magnetic surface variation experiments/Multiple pellet injection experiments. In: *Proc. 1st Int. Toki Conf. on Plasma Physics and Controlled Nuclear Fusion*, Toki, Report NIFS-PROC-3, National Institute for Fusion Science, Nagoya, pp. 196–199.
- Sudo, S. *et al.* (1990b). Scalings of energy confinement and density limit in stellarator/heliotron devices. *Nucl. Fusion* **30**, 11–21.
- Sudo, S. *et al.* (1990c). Plasma diagnostics in infrared and far-infrared range for Heliotron E. In: *Proc. 17th European Conf. on Controlled Fusion and Plasma Physics*, Amsterdam, Europhysics Conf. Abstracts, Vol. 14B, part IV, pp. 1524–1527.
- Talmadge, J.N. *et al.* (1989). Convective transport due to poloidal electric fields during electron cyclotron heating in IMS. *Nucl. Fusion* **29**, 1806–1810.
- Uchino, K. *et al.* (1988). Studies of particle behavior in Heliotron E by means of Balmer-alpha laser fluorescence spectroscopy. *J. Phys. Soc. Jpn.* **57**, 909–917.
- Yamada, H. (1990). private communication, National Institute for Fusion Science, Nagoya, Japan.

INTERNAL DISTRIBUTION

- | | |
|---------------------|--------------------------------------|
| 1. C. C. Baker | 18. T. E. Shannon |
| 2. L. A. Berry | 19. D. W. Swain |
| 3. B. A. Carreras | 20. N. A. Uckan |
| 4. R. A. Dory | 21. J. Sheffield |
| 5. J. L. Dunlap | 22-23. Laboratory Records Department |
| 6. W. Fulkerson | 24. Laboratory Records, ORNL-RC |
| 7. J. H. Harris | 25. Central Research Library |
| 8. H. H. Haselton | 26. Document Reference Section |
| 9. R. C. Isler | 27. Fusion Energy Division Library |
| 10. M. S. Lubell | 28-29. Fusion Energy Division |
| 11-15. J. F. Lyon | Publications Office |
| 16. M. Murakami | 30. ORNL Patent Office |
| 17. M. J. Saltmarsh | |

EXTERNAL DISTRIBUTION

31. Office of the Assistant Manager for Energy Research and Development, U.S. Department of Energy, Oak Ridge Operations Office, P. O. Box E, Oak Ridge, TN 37831
32. J. D. Callen, Department of Nuclear Engineering, University of Wisconsin, Madison, WI 53706-1687
33. R. W. Conn, Department of Chemical, Nuclear, and Thermal Engineering, University of California, Los Angeles, CA 90024
34. N. A. Davies, Acting Director, Office of Fusion Energy, Office of Energy Research, ER-50 Germantown, U.S. Department of Energy, Washington, DC 20545
35. S. O. Dean, Fusion Power Associates, Inc., 2 Professional Drive, Suite 248, Gaithersburg, MD 20879
36. H. K. Forsen, Bechtel Group, Inc., Research Engineering, P. O. Box 3965, San Francisco, CA 94119
37. J. R. Gilleland, L-644, Lawrence Livermore National Laboratory, P.O. Box 5511, Livermore, CA 94550
38. R. W. Gould, Department of Applied Physics, California Institute of Technology, Pasadena, CA 91125
39. R. A. Gross, Plasma Research Laboratory, Columbia University, New York, NY 10027

40. D. M. Meade, Princeton Plasma Physics Laboratory, P.O. Box 451, Princeton, NJ 08543
41. M. Roberts, International Programs, Office of Fusion Energy, Office of Energy Research, ER-52 Germantown, U.S. Department of Energy, Washington, DC 20545
42. W. M. Stacey, School of Nuclear Engineering and Health Physics, Georgia Institute of Technology, Atlanta, GA 30332
43. D. Steiner, Nuclear Engineering Department, NES Building, Tibbetts Avenue, Rensselaer Polytechnic Institute, Troy, NY 12181
44. R. Varma, Physical Research Laboratory, Navrangpura, Ahmedabad 380009, India
45. Bibliothek, Max-Planck Institut für Plasmaphysik, Boltzmannstrasse 2, D-8046 Garching, Federal Republic of Germany
46. Bibliothek, Institut für Plasmaphysik, KFA Jülich GmbH, Postfach 1913, D-5170 Jülich, Federal Republic of Germany
47. Bibliothek, KfK Karlsruhe GmbH, Postfach 3640, D-7500 Karlsruhe 1, Federal Republic of Germany
48. Bibliothèque, Centre de Recherches en Physique des Plasmas, Ecole Polytechnique Fédérale de Lausanne, 21 Avenue des Bains, CH-1007 Lausanne, Switzerland
49. R. Aymar, CEN/Cadarache, Département de Recherches sur la Fusion Contrôlée, F-13108 Saint-Paul-lez-Durance Cedex, France
50. Bibliothèque, CEN/Cadarache, F-13108 Saint-Paul-lez-Durance Cedex, France
51. Library, AEA Fusion, Culham Laboratory, Abingdon, Oxfordshire, OX14 3DB, England
52. Library, JET Joint Undertaking, Abingdon, Oxfordshire OX14 3EA, England
53. Library, FOM-Instituut voor Plasmafysica, Rijnhuizen, Edisonbaan 14, 3439 MN Nieuwegein, The Netherlands
54. Library, National Institute for Fusion Science, Chikusa-ku, Nagoya 464-01, Japan
55. Library, International Centre for Theoretical Physics, P.O. Box 586, I-34100 Trieste, Italy
56. Library, Centro Ricerca Energia Frascati, C.P. 65, I-00044 Frascati (Roma), Italy
57. Library, Plasma Physics Laboratory, Kyoto University, Gokasho, Uji, Kyoto 611, Japan
58. Plasma Research Laboratory, Australian National University, P.O. Box 4, Canberra, A.C.T. 2601, Australia
59. Library, Japan Atomic Energy Research Institute, Naka Fusion Research Establishment, 801-1 Mukoyama, Naka-machi, Naka-gun, Ibaraki-ken, Japan
60. G. A. Eliseev, I. V. Kurchatov Institute of Atomic Energy, P. O. Box 3402, 123182 Moscow, U.S.S.R.

61. V. A. Glukhikh, Scientific-Research Institute of Electro-Physical Apparatus, 188631 Leningrad, U.S.S.R.
62. I. Shpigel, Institute of General Physics, U.S.S.R. Academy of Sciences, Ulitsa Vavilova 38, Moscow, U.S.S.R.
63. D. D. Ryutov, Institute of Nuclear Physics, Siberian Branch of the Academy of Sciences of the U.S.S.R., Sovetskaya St. 5, 630090 Novosibirsk, U.S.S.R.
64. O. S. Pavlichenko, Kharkov Physical-Technical Institute, Academical St. 1, 310108 Kharkov, U.S.S.R.
65. Deputy Director, Southwestern Institute of Physics, P.O. Box 15, Leshan, Sichuan, China (PRC)
66. Director, The Institute of Plasma Physics, P.O. Box 26, Hefei, Anhui, China (PRC)
67. R. A. Blanken, Experimental Plasma Research Branch, Division of Applied Plasma Physics, Office of Fusion Energy, Office of Energy Research, ER-542, Germantown, U.S. Department of Energy, Washington, DC 20545
68. R. A. E. Bolton, IREQ Hydro-Quebec Research Institute, 1800 Montee Ste-Julie, Varennes, P.Q. JOL 2P0, Canada
69. D. H. Crandall, Experimental Plasma Research Branch, Division of Applied Plasma Physics, Office of Fusion Energy, Office of Energy Research, ER-542, Germantown, U.S. Department of Energy, Washington, DC 20545
70. R. L. Freeman, General Atomics, P.O. Box 85608, San Diego, CA 92138-5608
71. K. W. Gentle, RLM 11.222, Institute for Fusion Studies, University of Texas, Austin, TX 78712
72. R. J. Goldston, Princeton Plasma Physics Laboratory, P.O. Box 451, Princeton, NJ 08543
73. J. C. Hosea, Princeton Plasma Physics Laboratory, P.O. Box 451, Princeton, NJ 08543
74. R. Dagazian, Division of Confinement Systems, Office of Fusion Energy, Office of Energy Research, ER-55, Germantown, U.S. Department of Energy, Washington, DC 20545
75. R. H. McKnight, Experimental Plasma Research Branch, Division of Applied Plasma Physics, Office of Fusion Energy, Office of Energy Research, ER-542, Germantown, U.S. Department of Energy, Washington, DC 20545
76. E. Oktay, Division of Confinement Systems, Office of Fusion Energy, Office of Energy Research, ER-55, Germantown, U.S. Department of Energy, Washington, DC 20545
77. D. Overskei, General Atomics, P.O. Box 85608, San Diego, CA 92138-5608
78. R. R. Parker, Plasma Fusion Center, NW 16-288, Massachusetts Institute of Technology, Cambridge, MA 02139
79. W. L. Sadowski, Fusion Theory and Computer Services Branch, Division of Applied Plasma Physics, Office of Fusion Energy, Office of Energy Research, ER-541, Germantown, U.S. Department of Energy, Washington, DC 20545

80. J. W. Willis, Division of Confinement Systems, Office of Fusion Energy, Office of Energy Research, ER-55, Germantown, U.S. Department of Energy, Washington, DC 20545
81. A. P. Navarro, Division de Fusion, CIEMAT, Avenida Complutense 22, E-28040 Madrid, Spain
82. Laboratory for Plasma and Fusion Studies, Department of Nuclear Engineering, Seoul National University, Shinrim-dong, Gwanak-ku, Seoul 151, Korea
83. J. L. Johnson, Plasma Physics Laboratory, Princeton University, P.O. Box 451, Princeton, NJ 08543
84. L. M. Kovrizhnykh, Institute of General Physics, U.S.S.R. Academy of Sciences, Ulitsa Vavilova 38, 117924 Moscow, U.S.S.R.
85. T. Obiki, Plasma Physics Laboratory, Kyoto University, Gokasho, Uji, Kyoto, Japan
86. A. Iiyoshi, National Institute for Fusion Science, Chikusa-ku, Nagoya 464-01, Japan
87. V. D. Shafranov, I. V. Kurchatov Institute of Atomic Energy, P.O. Box 3402, 123182 Moscow, U.S.S.R.
88. J. L. Shohet, Torsatron/Stellarator Laboratory, University of Wisconsin, Madison, WI 53706
89. G. Grieger, Max-Planck Institut für Plasmaphysik, D-8046 Garching, Federal Republic of Germany
90. K. Matsuoka, National Institute for Fusion Science, Chikusa-ku, Nagoya 464-01, Japan
91. F. L. Ribe, University of Washington, Aerospace and Energetics Research Program, Mail Stop FL-10, Seattle, WA 98915
92. D. G. Swanson, Auburn University, Department of Physics, Auburn, AL 36849
93. R. K. Linford, Los Alamos National Laboratory, MS F646, P.O. Box 1663, Los Alamos, NM 87545
94. K. I. Thomassen, L-637, Lawrence Livermore National Laboratory, P.O. Box 5511, Livermore, CA 94550
95. R. F. Gandy, Physics Department, Auburn University, Auburn, AL 36849
96. H. Wobig, Max-Planck Institut für Plasmaphysik, D-8046 Garching, Federal Republic of Germany
97. D. T. Anderson, University of Wisconsin, Madison, WI 53706
98. K. Kondo, Plasma Physics Laboratory, Kyoto University, Gokasho, Uji, Kyoto, Japan
99. F. Sano, Plasma Physics Laboratory, Kyoto University, Gokasho, Uji, Kyoto, Japan
- 100-152. Given distribution as shown in OSTI-4500, Magnetic Fusion Energy (Category Distribution UC-426)